Air quality impacts of COVID-19 lockdown measures detected from space using high spatial resolution observations of multiple trace gases from Sentinel-5P/TROPOMI

Pieternel F. Levelt[1,2], Deborah C. Stein Zweers[1], Ilse Aben[3], Maite Bauwens[4], Tobias Borsdorff[3], Isabelle De Smedt[4], Henk J. Eskes[1], Christophe Lerot[4], Diego G. Loyola[5], Fabian Romahn[5], Trissevgeni Stavrakou[4], Nicolas Theys[4], Michel Van Roozendael[4], J. Pepijn Veefkind[1,2], Tijl Verhoelst[4]

[1]Royal Netherlands Meteorological Institute (KNMI), De Bilt, 3731GA, The Netherlands
[2]University of Technology Delft (TU Delft), Delft, 2628 CN, the Netherlands
[3]Netherlands Institute for Space Research (SRON), Utrecht, 3584 CA, The Netherlands
[4]Royal Belgian Institute for Space Aeronomy (BIRA-IASB), Brussels, 1180, Belgium
[5]German Aerospace Centre (DLR), Oberpfaffenhofen, Wessling, 82234, Germany

Correspondence to: Deborah C. Stein Zweers (stein@knmi.nl)

Abstract. The aim of this paper is to highlight how TROPOMI trace gas data can best be used and interpreted to understand event-based impacts on air quality from regional to city-scales around the globe. For this study, we present the observed changes in the atmospheric column amounts of five trace gases (NO_2, SO_2, CO, HCHO and CHOCHO) detected by the Sentinel-5P TROPOMI instrument, driven by reductions of anthropogenic emissions due to COVID-19 lockdown measures in 2020. We report clear COVID-19-related decreases in TROPOMI NO_2 column amounts on all continents. For megacities, reductions in column amounts of tropospheric NO_2 range between 14% and 63%. For China and India supported by NO_2 observations, where the primary source of anthropogenic SO_2 is coal-fired power generation, we were able to detect sector-specific emission changes using the SO_2 data. For HCHO and CHOCHO, we consistently observe anthropogenic changes in two-week averaged column amounts over China and India during the early phases of the lockdown periods. That these variations over such a short time scale are detectable from space, is due to the high resolution and improved sensitivity of the TROPOMI instrument. For CO, we observe a small reduction over China which is in concert with the other trace gas reductions observed during lockdown, however large, interannual differences prevent firm conclusions from being drawn. The joint analysis of COVID-19 lockdown-driven reductions in satellite observed trace gas column amounts, using the latest operational and scientific retrieval techniques for five species concomitantly is unprecedented. However, the meteorologically and seasonally driven variability of the five trace gases does not allow for drawing fully quantitative conclusions on the reduction of anthropogenic emissions based on TROPOMI observations alone. We anticipate that in future, the combined use of inverse modelling techniques with the high spatial resolution data from S5P/TROPOMI for all observed trace gases presented here, will yield a significantly improved sector-specific, space-based analysis of the impact of COVID-19 lockdown measures as compared to other existing satellite observations. Such analyses will further enhance the scientific impact and societal relevance of the TROPOMI mission.

Key words: Air quality, Trace gases, Sentinel-5P, TROPOMI, COVID-19, emissions

1   Introduction

In an effort to limit the transmission of the SARS-CoV-2 virus responsible for the Coronavirus disease 2019 (hereafter referred as COVID-19), drastic lockdown measures were implemented around the globe in the first half of 2020. These policies led to dramatic reductions in human activity, especially in the transport and industrial sectors, resulting in large decreases in the concentration of air pollutants (Bauwens et al., 2020; Shi and Brasseur, 2020; Forster et al., 2020; Diamond and Wood, 2020; Kroll et al., 2020; Le Quéré et al., 2020; Guevara et al., 2021; Gkatzelis et al., 2021). These changes were observed over China as early as February 2020 (Bauwens et al., 2020; Liu et al., 2020; Zhang, Z. et al., 2020; Zhao, N. et al., 2020) and were detected later in many other countries as similar lockdown measures were adopted (Bauwens et al., 2020; Broomandi et al., 2020; Collivignarelli et al., 2020; Lee et al., 2020; Gkatzelis et al., 2021; Koukouli et al., 2021).

The TROPOspheric Monitoring Instrument (TROPOMI; Veefkind et al., 2012; Ludewig et al., 2020) on board the European Copernicus Sentinel-5 Precursor (S5P) satellite, launched on 13 October 2017, is specifically designed for tropospheric monitoring on the global scale and has a daily revisit time. Compared to its predecessor OMI, TROPOMI's highest spatial resolution (3.5×5.5 km^2) is about 16 times better and its signal-to-noise ratio per ground pixel is substantially higher. This results in a large improvement in measurement sensitivity for relevant air quality products, including NO_2, SO_2, HCHO, and CHOCHO, thus enabling the study of rapid emission changes for even smaller sources as compared to previous instruments. For CO measurements, the daily global coverage of TROPOMI at a resolution of 7×5.5 km^2 represents a huge improvement to its predecessor SCIAMACHY (Bovensmann et al., 1999; Borsdorff et al., 2016; Borsdorff et al., 2017) with a spatial resolution of 120×30 km^2.

The observations from TROPOMI thus provide a unique opportunity to observe the magnitude and timing of the changes in tropospheric trace gas constituents, resulting from unprecedented COVID-19 lockdown measures. The initial TROPOMI observations of dramatic reductions in NO_2 column amount over regions with strictly enforced lockdowns, over China in particular, triggered a high level of interest worldwide, and initiated a large number of studies, mainly aimed at regional scales and largely focused on NO_2. However, the unparalleled capacity of TROPOMI to provide relevant information on COVID-19 driven emission reductions based on multiple species measurements has not been exploited yet. The objective of this work is to investigate the COVID-19 driven changes in the column amounts of five trace gases (NO_2, SO_2, CO, HCHO, and CHOCHO) from the global level down to individual cities using state-of-the-art TROPOMI operational and scientific data products. More specifically, we aim to

1. Summarize the analysis of tropospheric NO_2 at city-scale for all continents.

A large body of studies investigated the impact of the COVID-19 lockdowns on NO_2 concentrations (e.g. Bauwens et al., 2020; Baldasano, 2020; Huang et al., 2020), at regional and continental scale. Here, we analyze the time series of NO_2 measurements from a single satellite instrument for globally distributed locations on regional to city scales. In doing so, we further demonstrate the unique capabilities of how the TROPOMI instrument can be used to consistently track changes in air quality and anthropogenic emissions across the globe.

2. Explore the high spatial resolution and simultaneous TROPOMI observations of NO_2, SO_2, CO, HCHO, and CHOCHO.

73 While all of these gases have significant anthropogenic sources, they differ in their relative contribution to the energy,
74 industry, and transport sector emissions, and each sector exhibits a different response to COVID-19 lockdown
75 measures. Therefore, the combination of several TROPOMI trace gas products contains additional information on
76 sector-specific emissions and COVID-19 lockdown-induced changes in atmospheric composition. We show that
77 meaningful trends and source detection can be obtained by using the high spatial resolution of TROPOMI data and by
78 averaging that data over relatively short time periods. Although this is in large part the result of the improved
79 sensitivity of the instrument, we also introduce new developments in trace gas retrieval techniques and ad-hoc
80 corrections to enhance the sensitivity of the TROPOMI datasets to even smaller emissions and smaller changes in
81 emissions. In order to achieve these goals, we discuss the strengths and limitations of each of the retrievals for tracking
82 global to city-scale changes.

83 In the next section, the TROPOMI data will first be described in general terms, followed by a description per species
84 to address the retrieval methods, as well as a description of how we handle each data product in this study. The goal
85 of this methods and data section is not only to explain how this study was conducted but also to provide guidance to
86 data users on how to best interpret and analyze TROPOMI trace gas data not only for lockdown-driven emission
87 changes but also for other event-driven changes. This will be followed by a context-setting section reviewing the
88 global and regional impacts of COVID-19 lockdown measures and city-scale effects for all continents, using
89 TROPOMI NO_2 data. The next two sections will describe the effect of the lockdown measures on a regional scale by
90 examining NO_2, SO_2, CO, HCHO, and CHOCHO for China and India. The last section will feature an outlook of
91 future applications for this type of analysis followed by conclusions.

2   Methods and Data

93 In this work, our analysis is primarily based on TROPOMI data for regional lockdown periods in 2020 as compared
94 to the same periods in 2019 and will be presented in the broader context of the TROPOMI operational data record,
95 which started on 30 April 2018. We make use of observations from the TROPOMI instrument on board S5P which is
96 a push-broom imaging spectrometer (Veefkind et al., 2012) measuring in the ultraviolet (UV), visible (VIS), near-
97 infrared (NIR), and shortwave infrared (SWIR) spectral bands selected to measure the absorption by a large number
98 of trace atmospheric constituents as well as by clouds and aerosols. Using the spectral radiance measurements from
99 TROPOMI, atmospheric column amounts of different gases are retrieved as well as cloud and aerosol properties. For
100 this work, we use the following TROPOMI data products: NO_2, SO_2, CO, HCHO and CHOCHO as summarized in
101 Table 1. We did not include the following TROPOMI data products: tropospheric ozone columns, due to the tropics-
102 only spatial coverage; methane, due to an even longer atmospheric lifetime than CO where its sources were not as
103 impacted by lockdown measures; and aerosol index, designed to highlight long-range transported and/or elevated
104 plumes of smoke, dust, and/or ash and which is not a quantitative measure of aerosol amount nor sensitive to near-
105 surface emissions.

106 The S5P satellite flies in a Sun-synchronous orbit, with a local overpass time of 13:30. TROPOMI has a 2600 km
107 wide swath, providing near-daily global coverage. The spatial sampling of TROPOMI varies over the spectral bands.
108 The nadir sampling at the start of the operational period on 30 April 2018 was approximately 3.5 x 7 km^2 (across- x

109 along-track) for the ultraviolet and visible bands, and 7 x 7 km^2 in the shortwave infrared band. On 6 August 2019,

110 after implementation of a modified co-adding scheme, the sampling for these bands was improved to 3.5 x 5.5 km^2

111 and 7 x 5.5 km^2, respectively.

112   TROPOMI observations are being widely used within and beyond the scientific community and so it is crucial to

113 provide information on how these observations can best be used, interpreted, and analyzed. The COVID-19 lockdown

114 periods provide a unique use-case for the TROPOMI lead algorithm developers to highlight important differences in

115 the individual atmospheric lifetime and detectability of each trace gas and show how these characteristics are key to

116 the interpretation of the concomitant observations. It is not sufficient, for example, to illustrate lockdown-driven

117 changes in emissions simply by selecting a single day or week of TROPOMI column data for a given region as

118 measured during a lockdown period to the same day or week from year(s) prior (Braaten et al., 2020). We go further

119 to address the importance of delineating meteorological and seasonal variability from lockdown-driven changes in

120 emissions.

121   Therefore, we start this methods and data section with a general overview of considerations for the data user to take

122 into account for analyses aimed at the quantification of changes in the emission of these trace gases. Next, in dedicated

123 subsections, we provide a summary of the most relevant documentation and retrieval methods employed for each trace

124 gas (see Table A1). Even though each retrieval is based on the analysis of the amount of trace gas specific absorption

125 in measured radiance spectra, methods differ significantly per species.

126 **2.1   Understanding and Interpreting TROPOMI trace gas retrievals**

127 For this paper we will focus on TROPOMI trace gas retrievals for NO_2, SO_2, CO, HCHO, and CHOCHO (See Table

128 1). To understand and interpret the TROPOMI measurements of these trace gas species and how they vary with respect

129 to COVID-19 lockdown measures, it is necessary to consider their sources, variability through the atmospheric

130 column, and their atmospheric lifetimes. Although the mechanisms for the emission of each gas are different, there

131 are several common anthropogenic emission sources, most notably from transportation and industry, as listed in Table

132 1 which were significantly impacted by lockdown measures.

133

134 **Table 1: Summary of the retrieval spectral range, atmospheric lifetime, and main emission sources, for each trace gas**
135 **addressed in this study.**

Trace Gas Data Product Type (retrieval reference)	Spectral Range	Typical lifetime	Main emission sources
NO_2 Operational (van Geffen et al., 2019)	405-465 nm	2 to 12 hours	- Transportation - Industry - Power generation - Biomass burning
SO_2 Prototype (Theys et al., 2021)	310.5-326 nm	6 hours to several days	- Power generation - Industry - Transportation - Volcanoes[1]

CO Operational (Landgraf et al., 2016)	2324–2338 nm	Weeks to a month	- Transportation - Residential cooking and heating - Industry - Biomass burning - Oxidation of biogenic hydrocarbons - Methane Oxidation - Power generation
HCHO Operational (De Smedt et al., 2018)	328.5-359 nm	Several hours (lifetime of NMVOC precursors up to several days)	Primary and secondary product (NMVOC precursors) from: - Biogenic emissions - Biomass burning - Transportation - Industry
CHOCHO Prototype (Lerot et al., 2020)	435-460 nm	Several hours (lifetime of NMVOC precursors up to several days)	Primary and secondary product (NMVOC precursors) from: - Biogenic emissions - Biomass burning - Transportation - Industry

136 [1]Volcanic emissions are not significant for this work.

137

138   A brief evaluation of how the sources of these trace gases were or were not affected by lockdown-driven changes
139   lends insight into expected changes. In general, primary production trace gases, like NO_2 and SO_2 with relatively short
140   atmospheric lifetimes exhibit emission changes most clearly and rapidly. Although NO_2 and SO_2 are both important
141   primary production anthropogenic pollutants, their sectoral sources are different. For instance, the impact of lockdown
142   on the transportation sector is expected to have a bigger impact on NO_2 than SO_2, since this sector is responsible for
143   about 30% of the global NO_x emissions and only 1% of the global SO_2 emissions, according to the CAMS-ANT
144   inventory (Granier et al., 2019). On the other hand, SO_2 emissions are more likely to be impacted by possible changes
145   in power generation, since this sector accounts for 52% of the global SO_2 emissions and only 30% of the global NO_x
146   emission (Granier et al., 2019).
147   For CO, secondary production by methane oxidation and the oxidation of (biogenic) hydrocarbons accounts for at
148   least 60% of the total atmospheric CO, followed by contributions from biomass burning and fossil fuel use (Müller et
149   al., 2018; Holloway et al., 2000). Anthropogenic CO emissions originate from the industry, transportation, and
150   residential sectors and account for about 30% of the global emissions (Granier et al., 2019). However, it is noted that
151   the relative contribution of these sources varies per global region (Janssens-Maenhout et al., 2015). Although local
152   impacts of lockdown are likely for locations with strong anthropogenic CO emissions, overall a much smaller
153   lockdown-driven impact is expected for CO based on its longer atmospheric lifetime and smaller contributions from
154   lockdown affected sources (Clark et al., 2021).

Both HCHO and CHOCHO are short-lived indicators of non-methane volatile organic compound (NMVOC) emissions resulting from biogenic processes, large biomass burning events, and anthropogenic activities (Millet et al., 2008; Fu et al., 2008; Stavrakou et al., 2009; Bauwens et al., 2016; Chan Miller et al., 2016). They are mostly produced as secondary products from oxidation of other NMVOCs but are also directly emitted from combustion and industrial processes, although to a lesser extent. In general, the relative production of CHOCHO from such combustion processes and from the oxidation of aromatics, originating mostly from the industrial sector, is higher than for HCHO. Thus, the CHOCHO response to changes in anthropogenic emissions is expected to be stronger (Chan Miller et al., 2016; Cao et al., 2018).

It is important to note that the retrievals provide information on the tropospheric or total column amount of these gases, because the spectra contain limited information on their vertical distribution in the atmosphere. TROPOMI observations thus provide a two-dimensional representation of the three-dimensional atmosphere. The vertical profiles of each trace gas vary significantly depending on the injection height of the emissions and atmospheric lifetime (see Table 1). For example, NOx emissions at the surface result in NO_2 vertical profiles that peak in the near-surface layer (lowest 1-2 km of the troposphere), due to the short lifetime of NO_2. Similarly, SO_2 has a vertical profile which generally peaks in the lower troposphere. CO on the other hand, has a lifetime of weeks to a month (depending on the reaction with the hydroxyl radical) and can be transported over great distances, both horizontally and vertically. Therefore, CO even though it is often co-emitted with NO_2, has a significantly higher background concentration throughout the troposphere as compared to NO_2. HCHO and CHOCHO have lifetimes of a few hours but are generally formed in the atmosphere via secondary production processes, which leads to an intermediate profile shape as compared to NO_2 and CO.

In addition to vertical profiles that vary per trace gas species, the vertical sensitivity of the TROPOMI measurements also varies per species. For the trace gases retrieved in the UV and VIS ranges, the sensitivity decreases towards the surface so that the accuracy of the retrieved column depends on a well-characterized a priori knowledge of the vertical distribution. Due to scattering, the near-surface sensitivity is lower in the UV (SO_2, HCHO) than in the VIS (NO_2 and CHOCHO). In the SWIR range, the vertical sensitivity is more constant. As part of the retrieval process, a priori vertical profiles of each trace gas are scaled to match the measured tropospheric column. An uncertainty in the retrieved column amount or vertical column density (VCD) is associated with inherent differences between the true and a priori vertical profiles. However, the averaging kernels, which are reported in the data products, can be used to replace the a priori profiles with custom profiles (e.g. Eskes and Boersma, 2003; Eskes et al., 2020) thereby reducing the corresponding uncertainty. In this study, we mostly focus on relative changes in VCDs and use standard a priori profiles for each data product. Therefore, the uncertainty related to the vertical profile is rather small (as detailed in Sect. 2.2 through 2.6). Another contribution to this error is the use of partly cloudy scenes by each retrieval which increases the amount of data available but does change the vertical sensitivity. The cloud fraction threshold for each trace gas is described in Sect. 2.2 through 2.6. In future studies, the averaging kernels could be used for inversion modelling of emissions. As explained in Eskes and Boersma 2003, relative comparisons between the observations and the model used in the inverse modelling system, and therefore the resulting emissions, no longer depend on the retrieval a-priori profile shape when the kernel is applied to the model.

TROPOMI observes atmospheric concentrations of trace gases integrated over a vertical column, which is not the same as a direct measurement of the (near-surface) emission. The amount of a given trace gas integrated over a vertical column at a certain location depends not only on emission and deposition, but also on atmospheric transport and (photo)chemical reactions. Note that the background concentration is higher for trace gases with a longer atmospheric lifetime. In turn, enhanced background concentrations will increase the relative importance of atmospheric transport versus local emissions. Local NO_2 emissions have a relatively large impact on the measured column amounts, while for CO the contribution of remote sources can in some cases be superimposed on local emissions thus making the interpretation more difficult. To attribute a change in concentration to a corresponding change in local emissions, the effects of meteorology and chemical lifetime must be accounted for as well.

While emissions can be estimated from satellite observations using data-driven methods (Beirle et al., 2019, Beirle et al., 2021; Fioletov et al., 2016; Goldberg et al., 2019) or using complex inverse modelling techniques (e.g. Millet et al., 2008; Stavrakou et al., 2009; Bauwens et al., 2016; Ding et al., 2020; Miyazaki et al., 2020; Borsdorff et al., 2019; Borsdorff et al., 2020), here we use a more qualitative approach to probe emission changes. First we compare the column amounts in 2020 with those from the same period from earlier years and then carry out additional analysis to separate the lockdown-driven variability from seasonal and meteorological variability taking into account local information about lockdown and anticipated impacts from different source sectors.

2.2 Nitrogen dioxide (NO_2)

The tropospheric column of nitrogen dioxide (NO_2) is a TROPOMI operational data product (Veefkind et al., 2012; doi.org/10.5270/S5P-s4ljg54). Product versions are listed in the Product Readme File (PRF, Eskes and Eichmann, 2019a). The retrieval method is described in detail in the NO_2 Algorithm Theoretical Basis Document (ATBD, van Geffen et al., 2019). The data product and data usage are described in in the NO_2 Product User Manual (PUM, Eskes et al., 2020). The dataset used for most of NO_2 analyses cover the period from 1 January 2018 to 30 May 2020. For Europe, the dataset was extended through 31 August 2020.

The retrieval algorithm derives NO_2 information from spectral range 405-465 nm and is largely based on the OMI NO_2 retrieval developments implemented during the EU QA4ECV project (Boersma et al., 2018). The retrieval consists of three steps. The first step is based on the DOAS approach, in which the total slant column of NO_2 is retrieved from the TROPOMI spectra, as discussed in van Geffen et al. (2020). The second step is the estimation of the 3-D stratospheric distribution of NO_2 based on an assimilation of the TROPOMI slant column data of previous days using the chemistry-transport model TM5-MP (Williams et al., 2017) run at 1° x 1°. This assimilation is set up to predominantly make use of measurements over clean areas (e.g. ocean and remote land regions) with limited tropospheric NO_2. The third step is the conversion of the tropospheric slant column (total minus stratosphere) into a tropospheric vertical column by combining radiative transfer calculations with a priori profile shapes from the TM5-MP model. The data product is very comprehensive and provides all the input (such as surface and cloud information) and intermediate products.

The tropospheric column is delivered with corresponding averaging kernels and a detailed error estimate. The random error on the slant column is discussed in van Geffen et al. (2020), and is on the order of 0.56×10^{15} molec cm⁻

228   ^{2} for individual measurements after 6 August 2019 (for pixel size 3.5 x 5.5 km^2). This translates to only small random

229   errors in the total columns on the order of 0.2×10^{15} molec cm^{-2}. Uncertainties in the estimate of the local stratospheric

230   column amount is of the same order of magnitude. The uncertainty related to the computation of the air mass factor

231   (AMF) is much more significant for tropospheric columns over polluted areas. The AMF uncertainties are driven by

232   the treatment of surface albedo, clouds, aerosols, and profile shape. Such errors are multiplicative, and are of the order

233   of 20-60% depending on the geographical location, time of day, and season (van Geffen et al., 2021). These

234   uncertainties are modelled for individual observations and are provided in the data product.

235   As for all operational TROPOMI data products, a quality assurance value (qa_value) is provided to filter the data

236   and remove lower quality data where, the recommended threshold value depends on the application (see also Appendix

237   A, Table A1). For direct visualization or gridding applications a qa_value greater than 0.75 is recommended. For

238   comparisons with models and data assimilation through the use of the averaging kernels, a relaxed qa_value of greater

239   than 0.5 may be used. In this study we use NO$_2$ retrievals with a qa_value greater than 0.75. Application of this

240   qa_value threshold corresponds to data with mostly clear-sky conditions (cloud radiance fractions < 0.5) and implies

241   that the data is filtered to remove retrievals which do not meet certain quality criteria as described van Geffen et al.

242   (2019).

243   Several recent papers discuss the validation of the NO$_2$ product against independent observations (Verhoelst et al.,

244   2021; Tack et al., 2021; Judd et al., 2020; Dimitropoulou et al., 2020; Ialongo et al., 2020). The main findings can be

245   summarized as follows: the stratospheric and slant columns are in good overall agreement with other satellite

246   measurements (van Geffen et al., 2020) and with ground-based observations (Verhoelst et al., 2021). However, the

247   tropospheric column presents a negative bias of the order of 30% with respect to ground-based remote sensing

248   reference observations (Verhoelst et al., 2021; Dimitropoulou et al., 2020), as well as with imaging data from airborne

249   measurements (Judd et al., 2020; Tack et al., 2021). Although the origin of this bias remains unclear and may be due

250   to several causes, validation results indicate that it scales linearly with the retrieved tropospheric column amount

251   (Verhoelst et al., 2021; see Fig. C1). As a result, (COVID-related) relative changes in the NO$_2$ column, e.g., (2020-

252   2019)/2019, should be largely insensitive to this bias.

253   **2.3   Sulphur dioxide (SO$_2$)**

254   Initial analyses were performed using the TROPOMI operational data product for SO$_2$ (Theys et al., 2017). However,

255   biases present in those data (Fioletov et al., 2020) hamper the detection of the type of small changes in SO$_2$, typically

256   on the order of -0.1 DU, that are under investigation in this work. Therefore, an alternative retrieval scheme was

257   applied, the so-called COvariance-Based Retrieval Algorithm (COBRA; Theys et al., 2021). In brief, the approach

258   considers a set of SO$_2$-free spectra in the wavelength range 310.5-326.0 nm (from TROPOMI band 3) to represent the

259   radiance background variability, in the form of a covariance matrix. The latter is updated for each orbit, TROPOMI

260   row, and per latitude band. The covariance matrix is used to determine the SO$_2$ slant columns from individual spectral

261   measurements using an optimally weighted single parameter retrieval (see Walker et al., 2011). We note that COBRA

262   does not recalculate air mass factors (AMF). These are simply extracted from the operational product to convert SO$_2$

263   slant columns into vertical columns (VCDs). Compared to the operational DOAS results, COBRA significantly

264 improves the SO$_2$ VCDs, both in terms of precision and accuracy. Because the approach empirically accounts for all
265 sources of systematic variability in the measured signal, large-scale biases typically observed with the DOAS approach
266 are efficiently removed leading to a large gain in sensitivity (see Fig. C2).

267 In this study, we use SO$_2$ retrievals under clear-sky conditions (cloud fractions less than 30%) with solar zenith
268 angles lower than 60°, and we eliminate 25 swath edge pixels from each side of the orbit swath (450 pixels wide). The
269 random error in the SO$_2$ vertical columns is rather small in the range of 0.5-1.0 DU, and can be largely reduced by
270 data averaging. Errors due to spectral interferences are estimated to be very low, about 0.05 DU (Theys et al., 2021).
271 Remaining systematic uncertainties are mostly from the auxiliary data used in the AMF calculation, and are in the 30-
272 50% range. The dataset used for this analysis covers the period from May 2018 to June 2020.

2.4   Carbon monoxide (CO)

274 The total column of carbon monoxide (CO) is a TROPOMI operational data product obtained using TROPOMI 2.3
275 micron measurements (Veefkind et al., 2012; doi.org/10.5270/S5P-1hkp7rp). Product versions are listed in the Product
276 Readme File (Landgraf et al., 2020). The data product and data usage are described in in the CO Product User Manual
277 (Apituley et al., 2018). This CO retrieval uses the Shortwave Infrared CO retrieval (SICOR) algorithm method and is
278 described in detail in the CO Algorithm Theoretical Basis Document (Landgraf et al., 2018). The algorithm software
279 is based on a scattering forward model and retrieves trace gas columns simultaneously with effective cloud parameters
280 (cloud height, cloud optical thickness) from the SWIR channel to account for cloud contaminated measurements
281 (Landgraf et al., 2016, 2018). The inversion deploys a profile scaling approach by which a vertical CO reference
282 profile is scaled to obtain agreement between the forward simulation and the spectral measurement (Borsdorff et al.,
283 2014). The reference profile is based on a monthly averaged simulation from the global chemical transport model
284 TM5 and thus varies spatially and temporally (Krol et al., 2005). The vertical sensitivity of the retrieval for clear-sky
285 conditions is good throughout the atmosphere while measurements for cloudy conditions have reduced sensitivity
286 under the cloud (Borsdorff et al., 2018).

287 In this study, we use the CO retrieval for measurements under clear-sky and cloudy atmospheric conditions (cloud
288 altitude less than 5000m). This corresponds to filtering the dataset by using the quality assurance values (qa_value
289 greater than 0.5) that are supplied with the data product. CO retrievals under low cloud conditions perform well for
290 unpolluted scenes however can lead to e.g. lower CO values when pollution hot spots are present below the cloud due
291 to optical shielding and scattering (Borsdorff et al., 2018). Consequently, retrievals under cloudy conditions must be
292 considered with care, however they are essential to improve the data coverage especially over the oceans where clear-
293 sky measurements are hampered by the low reflectivity of water in the SWIR spectral range.

294 The CO retrieval skill lies well within the requirements of the TROPOMI mission (Veefkind et al., 2012) on accuracy
295 (< 15%) and precision (< 10%). This was shown by validation with ground-based FTIR measurements operated by
296 the Total Carbon Column Observing Network (TCCON). TROPOMI CO is biased high compared to TCCON by
297 about 6 ppb with a station to station variability of about 4 ppb (Borsdorff et al., 2018; Lambert et al., 2020). The
298 dataset used for this analysis covers the period from 1 January 2018 to 30 May 2020.

2.5   Formaldehyde (HCHO)

The tropospheric column of formaldehyde (HCHO) is a TROPOMI operational data product (Veefkind et al., 2012; doi:10.5270/S5P-tjlxfd2). Product versions are listed in the HCHO Product Readme File (De Smedt et al., 2020a). The data product and data usage are described in in the HCHO Product User Manual (PUM, Romahn et al., 2020). The TROPOMI HCHO retrieval algorithm has been fully described in De Smedt et al. (2018) and in the HCHO ATBD (De Smedt et al., 2020b). It is based on the DOAS method, and is directly inherited from the OMI QA4ECV product (https://doi.org/10.18758/71021031). The fit of the slant columns is performed in the spectral interval of 328.5-359.0 nm. Reference spectra are updated daily using an average of Earth radiances selected in the Equatorial Pacific region. The conversion from total slant to tropospheric vertical columns is performed using a look-up table of vertically resolved air mass factors calculated at 340 nm. A priori vertical profiles are provided by the TM5-MP daily forecast with a spatial resolution of 1 x 1 degree (Williams et al., 2017). Cloud properties are taken from the S5P operational product Cloud as Reflecting Boundary (CRB; Loyola et al., 2018). In order to correct for any remaining offset and striping due to instrumental artefacts or unknown misfits in the spectral retrieval, a background correction is applied based on HCHO slant columns selected in the emission-free Pacific Ocean. The background HCHO vertical column, due to the methane oxidation, is added using data from the TM5 model in the reference region. We use the quality assurance values (qa_value greater than 0.5) to filter out observations presenting a solar zenith angle larger than 70° or cloud fractions larger than 0.4.

The HCHO retrieval fulfils the requirements of the TROPOMI mission (Veefkind et al., 2012) on accuracy (40-80%) and precision ($12x10^{15}$ molec cm^{-2}). The precision of a single observation is estimated to be $5x10^{15}$ molec cm^{-2} in remote locations. The dispersion is naturally larger over polluted sites (from $7-10x10^{15}$ molec cm^{-2}). Validation using a global network of FTIR measurements indicates that TROPOMI HCHO columns present a negative bias over high emission sites (-30% for HCHO columns larger than $7.5x10^{15}$ molec cm^{-2}) and a positive bias for clean sites (+20% for HCHO columns lower than $2.5x10^{15}$ molec cm^{-2}) (Lambert et al., 2020; Vigouroux et al., 2020).

To characterize the HCHO interannual and seasonal variability, we have used the QA4ECV OMI dataset to construct a climatology based on recent years (2010-2018). This is justified the good agreement between OMI and TROPOMI HCHO columns which is better than 10% for most regions (Lambert et al., 2020). For our analysis, we use two-week averaged columns. This reduces the random uncertainty to about 10%.

One of the main drivers of the observed HCHO variability is temperature, which has a direct impact on NMVOC emissions and on the chemical production of HCHO (Stavrakou et al., 2018). It results in a strong correlation between HCHO columns and surface temperatures. For this paper, we correct the HCHO column amounts for this meteorological impact prior to using the data in the analyses. We introduce a temperature correction method (Zhu et al., 2017) based on data from OMI for 2005-2020, and from TROPOMI for 2018-2020. In brief, this correction entails fitting a second-order polynomial through daily HCHO columns reported as a function of the temperature. This temperature correction is performed for each region and on the OMI and TROPOMI time series separately. On this basis, the temperature-induced variations in HCHO are removed from the time series using local daily temperatures specified by ERA5-Land 2m meteorological datasets (Muñoz Sabater, 2019a; See Fig. C3). This correction is designed to minimize the impact of temperature fluctuations on the HCHO anomalies. Finally, a polynomial obtained using a

climatology of surface temperatures is added to the differential HCHO columns, in order to reintroduce the natural seasonal cycle, assuming the same temperature every year. These temperature-corrected HCHO columns are used throughout this paper. Note that the difference with uncorrected HCHO columns is generally small (less than 10%), but can be significant when looking for small effects such as those induced by COVID-19 related emission changes. The dataset used for this analysis covers the period from May 2018 to June 2020.

2.6 Glyoxal (CHOCHO)

Glyoxal (CHOCHO) is not one of the TROPOMI operational data products. For this study we used the prototype data product developed as part of the ESA S5p+I GLYRETRO project, which relies on scientific developments performed using the GOME-2 and OMI instruments (Lerot et al., 2010). The algorithm is described in detail in the GLYRETRO ATBD (Lerot et al., 2020). In brief, the retrieval approach consists of a DOAS-type spectral fit for the observed optical depth with reference absorption cross-sections for glyoxal and other absorbing species (NO_2, O_3, O_2-O_2, liquid water and water vapor, and the Ring effect) in the spectral interval of 435-460 nm to derive glyoxal slant column densities. The latter are converted into tropospheric columns using calculated air mass factors, after application of a background correction procedure aimed at reducing possible remaining (row-dependent) systematic biases. Air mass factors are calculated following the formulation of Palmer et al. (2001), which combines altitude-dependent air mass factors (or Box-AMFs) with a priori glyoxal concentration profiles. The Box-AMFs represent the instrumental sensitivity to changes in concentration at any altitude and are precomputed using the radiative transfer model VLIDORT v2.7 (Spurr and Christi, 2019), while the a priori profiles are provided by the MAGRITTE chemistry-transport model (Müller et al., 2018, 2019).

The glyoxal optical depth is very small ($< 5x10^{-4}$), which makes its retrieval very sensitive to instrumental noise and to interferences with spectral signatures of species absorbing more significantly in the same spectral region. The first factor introduces large random errors, in the range $6-10x10^{14}$ molec cm^{-2}, which can however be reduced by spatial-temporal averaging, that is, using multiple observations averaged time and/or space. Systematic uncertainties are dominated by spectral interferences, but also by uncertainties associated with the auxiliary data used as an input for the AMF calculation. These uncertainties are estimated to be $2-3x10^{14}$ molec cm^{-2} (~50% for source regions). To limit uncertainties related to cloud contamination, glyoxal observations are only provided for scenes with effective cloud fractions smaller than 20% (taken from the operational NO_2 product). As with HCHO, to account for seasonal and interannual variability, a climatology of OMI CHOCHO columns was built to further delineate sources of variability for glyoxal column amounts.

Validation of satellite glyoxal column observations is generally limited, mostly due to the scarcity of independent ground-based data. However, a preliminary validation based on a few MAX-DOAS stations in Asia and Europe, indicates that the satellite and ground instruments measure consistent glyoxal tropospheric column amounts with mean differences generally less than $2x10^{14}$ molec cm^{-2}, except in particular conditions such as low sun elevation or for stations that are frequently covered by clouds (Alvarado et al., 2020). The dataset used for this analysis covers the period from May 2018 to June 2020.

3   Global Observations of Nitrogen Dioxide

Numerous papers have shown that TROPOMI measurements of tropospheric NO_2 column amount are well-suited for detecting emission from a variety of anthropogenic sources including traffic, power plants, and industry (van der A et al., 2020; Goldberg et al., 2019). The atmospheric lifetime of NO_2 and its vertical profile shape dictate that the high spatial resolution measurements from TROPOMI can readily capture rapid week-to-week changes in near-surface emissions from COVID-19 impacted cities and point sources (Sekiya et al., 2021; Fioletov et al., 2021; Stavrakou et al., 2021; Gkatzelis et al., 2021). To give context and overview, the global distribution of tropospheric NO_2 based on an annual average for 2019 with an oversampling resolution of approximately 0.02° x 0.02° is illustrated in Figure 1. The high resolution of these measurements enables further zooming to the regional, suburban, and city scale providing detailed information about spatial distributions. Three further zoom-in cases for central Chile and its capital Santiago, for Paris, and for New Delhi are shown in Figure 1. These cases focus on a shorter periods coinciding with region-specific COVID-19 lockdowns (see Appendix B). Observed column amounts of NO_2 are compared to similar periods in 2019, which are chosen to be longer than the 2020 period in order to reduce the effects of natural variability. Strong reductions in the NO2 tropospheric column amounts are observed during lockdown periods (Bauwens et al., 2020; Barré et al., 2021; Griffin et al., 2020; Qu et al., 2021). Interestingly, further zoom in shows that the relative reduction is not uniform over a city, reflecting differences in the mix of source contributions for different quarters of a given city.
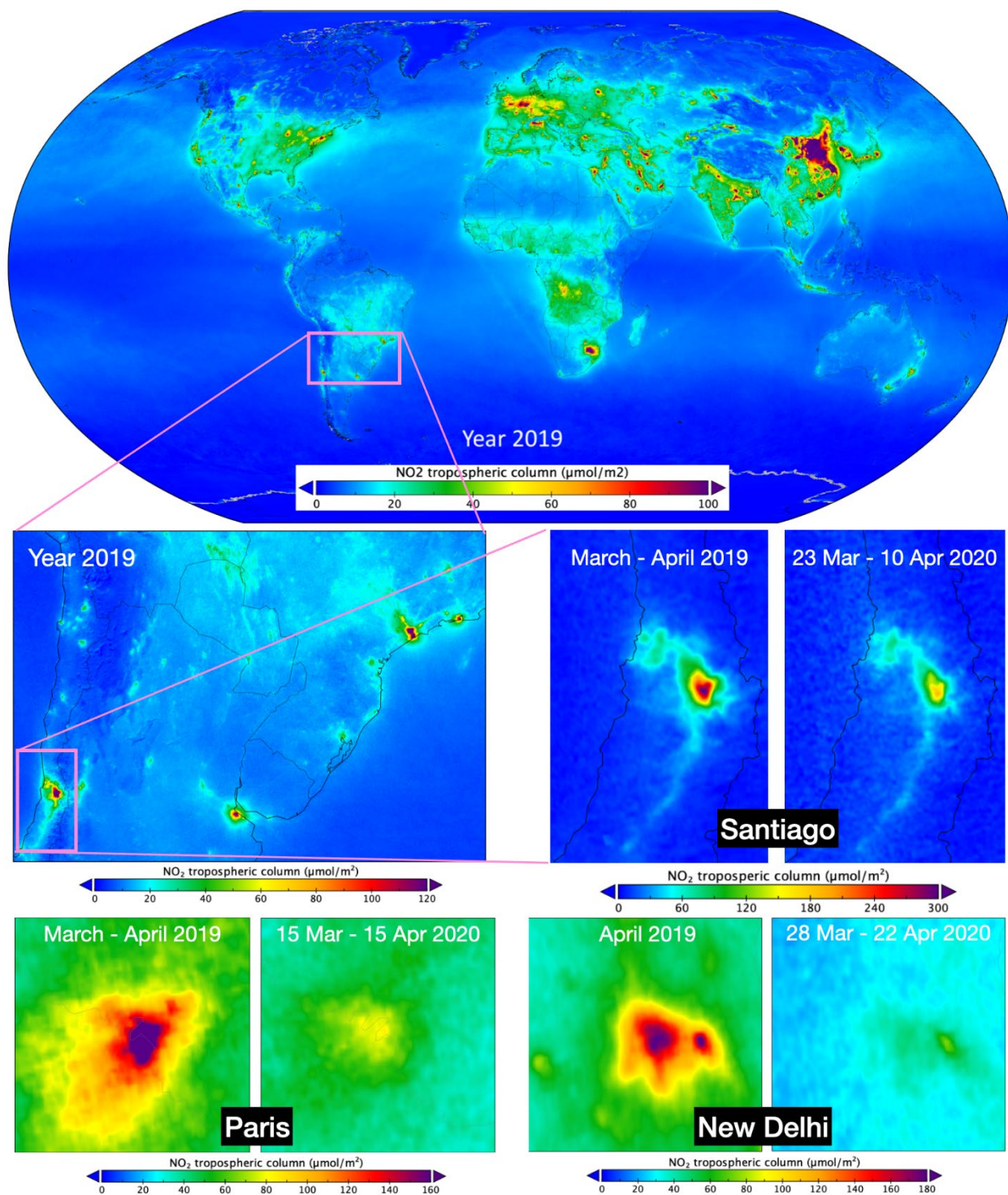
Figure 1: Global distribution of NO_2 based on the annual average of tropospheric column amounts of NO_2 measured by TROPOMI for 2019 (top panel) shown in units of micromole per m^2. Using the same data, several zoom-in plots are shown in the middle and bottom panels: regional zoom-in for central South America (middle left) and a city-scale zoom-in over Santiago, Chile (middle right panels, comparing 23 March to 10 April 2020 with March-April 2019), over Paris (lower left, comparing 15 March to 15 April 2020 with March-April 2019) and over New Delhi (lower right, comparing 28 March to 22 April 2020 with April 2019). Note the different color scales in the three subpanels. The domain size of the panels is 1.5 x 1.0 degree for Paris, and 1.1 x 1.0 degree for New Delhi.

399

400

The lockdown periods and the measures taken to mitigate the spread of COVID-19 were rolled out on country- and often city-specific basis. Figure 2 illustrates the temporal evolution of NO_2 tropospheric column amounts from January to May over large cities across different continents. The observed reductions in China and India are discussed in more detail in Sections 4 and 5. Detailed information about the lockdown measures adopted for those cities is given in Table B2. Appendix B provides a detailed description of the observed reductions during the specific lockdowns for individual (mega)cities shown in Figure 2 and Figure 3. The TROPOMI observations indicate substantial decreases in NO_2 during the lockdowns in all studied cities, but the reductions vary significantly from one city to another.

408

409
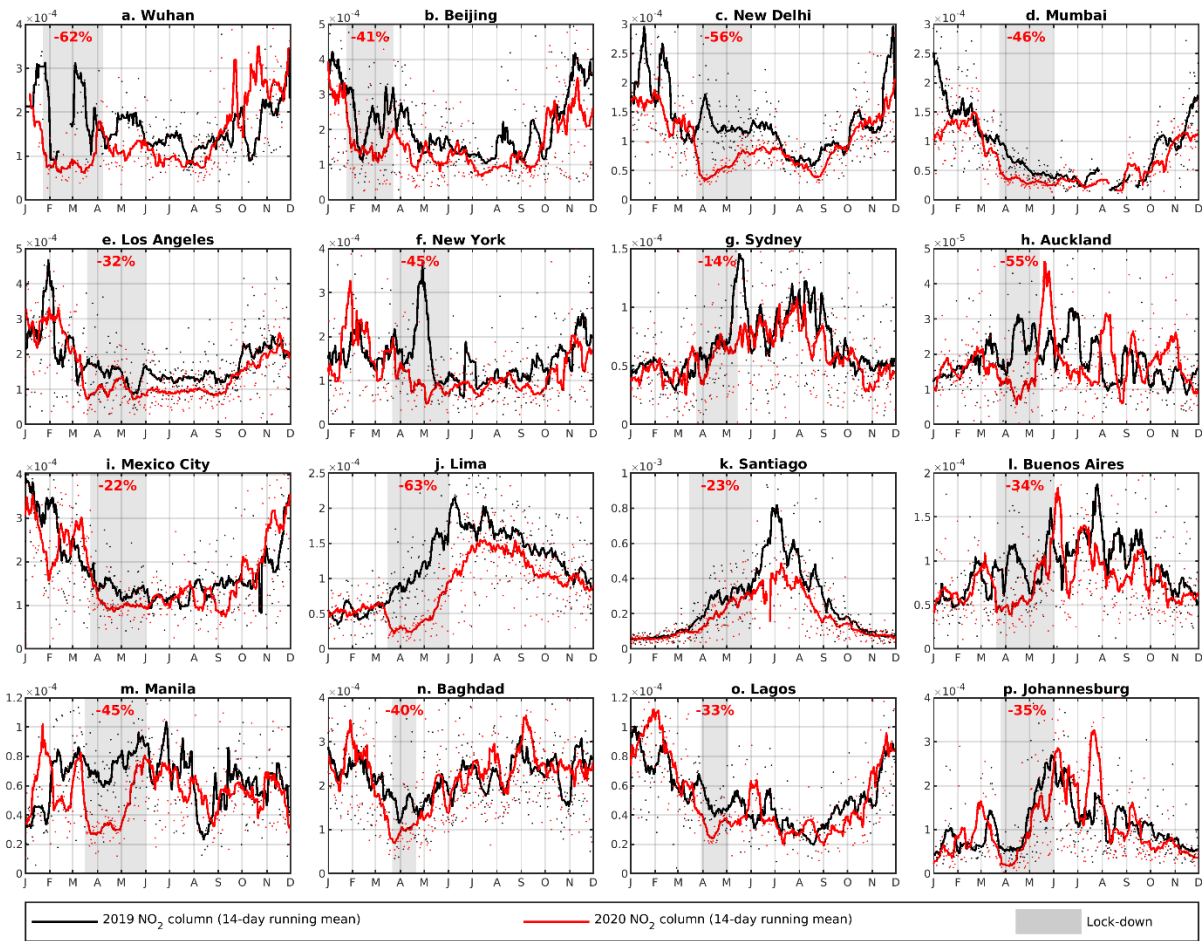
Figure 2: Time series of TROPOMI NO_2 column amounts (in mol m^{-2}) for selected cities for the period 1 January to 1 December in 2019 (black dots) and 2020 (red dots). TROPOMI observations are averaged over a 25 x 25km^2 box around the city center. The lines indicate the two-week running mean for 2019 (black) and 2020 (red). The grey zones indicate the official lockdown period for each city. The reduction of the average NO_2 column during the lockdown period relative to the same period in 2019 is given inset. Details about the lockdown dates are summarized in Table B2.

416
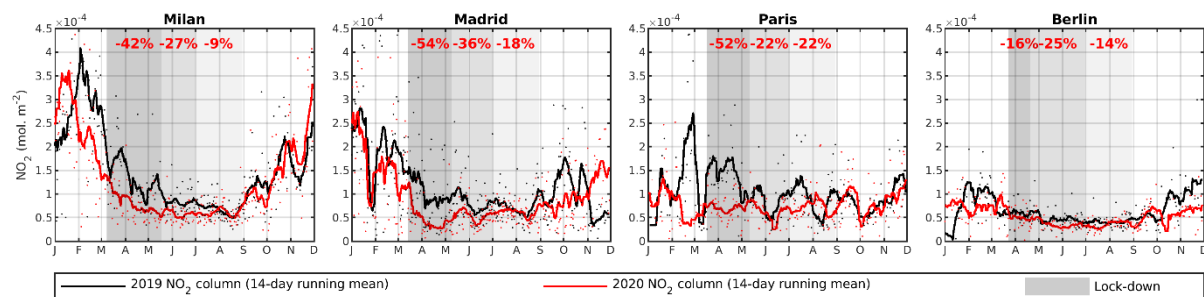
 Figure 3: Same as Figure 2, for the European cities Milan, Madrid, Paris, and Berlin, for the same period of 1 January to
 1 December in units of mol m^{-2}. Additional shading indicates the lockdown period (dark grey), a transition period (grey),
 and the period with relaxed regulations (light grey).
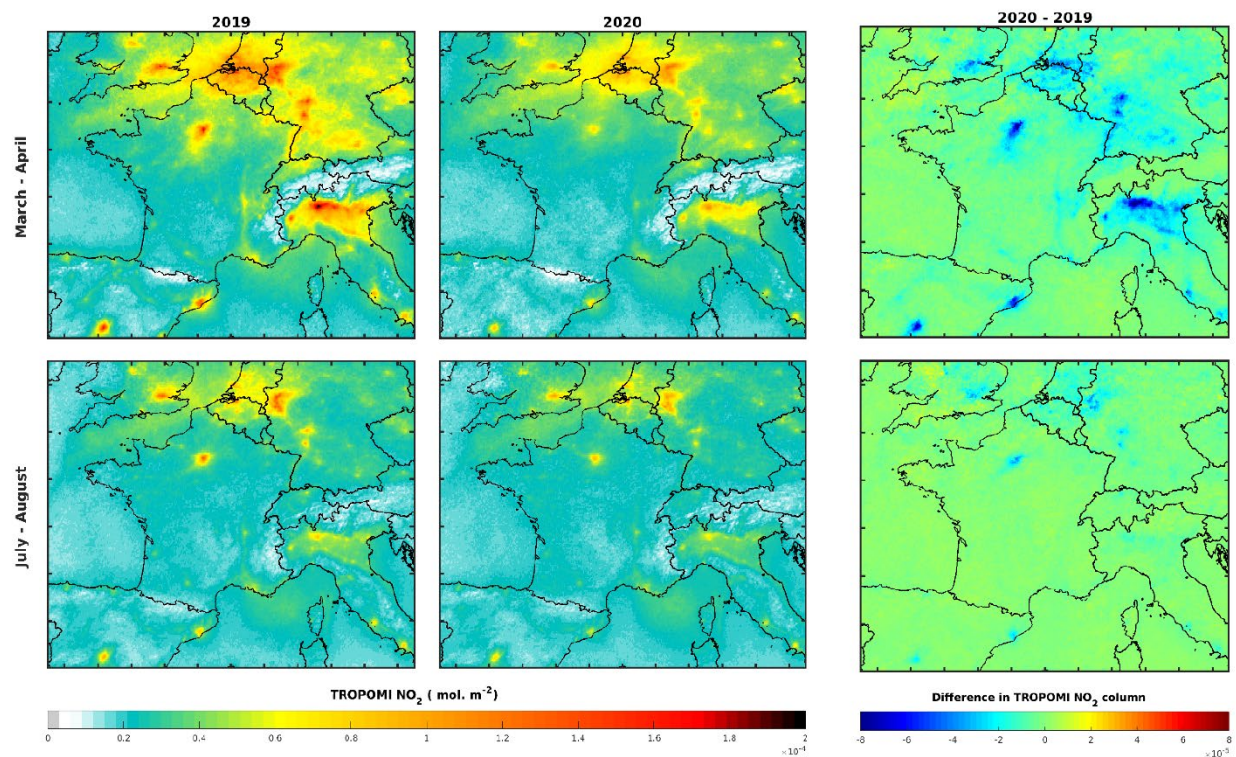
 Figure 4: TROPOMI NO$_2$ tropospheric columns over Europe in the lockdown months March-April (top) and the post-
 lockdown months July-August (bottom), comparing 2019 (left) with 2020 (middle) in units of mol m^{-2}. The difference is
 shown in the right panel.

 Relative concentration changes between 2019 and 2020 (as shown in Figure 4), as mentioned previously, should not

 be fully attributed to COVID-19 lockdown measures and the subsequent reduction of emissions. Daily changes in the

 weather have a strong influence on the NO$_2$ concentrations, even when the data is averaged over a month. In order to

 estimate the impact of meteorological variability on TROPOMI-based NO$_2$ observations, simulations were performed

with the LOTOS-EUROS chemistry-transport model over Europe at a resolution of 0.1° x 0.1°. Using the same emissions for 2019 and 2020, the simulations show that meteorological variability is responsible for changes in the monthly-mean, city-averaged NO_2 columns with a 1-sigma standard deviation of about 13%. This variability is clearly illustrated in e.g. the individual daily observations in Figure 2. The drastic changes in the range of 30-60% observed in the TROPOMI data and shown in Figure 1 through Figure 4 clearly fall outside this range and cannot be attributed to weather alone.

A second complication is the presence of clouds. Months with persistent local cloud cover will therefore have a reduced number of tropospheric column observations and will exhibit more natural variability. For quantitative estimates of the COVID-19 measures, these factors should be carefully taken into account. This can be done through (i) daily-based analysis of the NO_2 plumes from cities using wind speed fields from meteorological models and subsequent emission derivation (Lorente et al., 2019; Goldberg et al., 2019); (ii) combining NO_2 observations with analyzed wind fields (Beirle et al., 2019, 2021); (iii) regression models to estimate the impact of natural variability and emission trends in the observations (Diamond and Wood, 2020); (iv) chemistry-transport modelling (Chang et al., 2020; Liu et al., 2020; Barré et al., 2021); and (v) inverse modelling and data assimilation approaches (Ding et al., 2020; Miyazaki et al., 2020).

4 Regional Observations for China

China was the first country to impose measures to limit the spread of the SARS-CoV-2 virus. Although no national lockdown was declared, strict local lockdown measures were implemented in many cities and provinces. In Wuhan, the epicenter of the virus outbreak, the lockdown period lasted from 23 January 2020 until 8 April 2020, while in other regions, it generally started in early February with measures being eased and lifted through March. In addition to the lockdown measures, the yearly Chinese New Year holidays also affected the amount of anthropogenic emissions (Tan et al., 2009), and so needs to be considered for proper interpretation of the observations. The timing of the holiday period differs from year to year and took place from 24 January to 2 February in 2020, and in the periods 4-10 February and 15-21 February for 2019 and 2018, respectively.

The impact of the COVID-19 crisis on air quality in China has already been investigated in several studies. Bauwens et al. (2020) reported that tropospheric NO_2 column amounts observed by TROPOMI during the lockdown dropped by 40-50% in the most impacted cities compared to the same period in 2019 (see Sect. 3). Accordingly, top-down estimated NOx emissions exhibited sharp reductions of up to 50% during the strict lockdown period in late January through early February (Ding et al., 2020; Liu et al., 2020; Zhang, R. et al., 2020).

In situ data indicate significant reductions of ground concentrations for NO_2, but also for PM, SO_2, and CO (Shi and Brasseur, 2020; Wang et al., 2020; Zhang, Z. et al., 2020; Zhao, Y. et al., 2020). On the other hand, those studies consistently reported increases of ozone concentrations. With the support of models, Zhao, Y. et al. (2020) have shown that the observed decreases in NO_2 concentration were mostly caused by emissions reductions. They also show that the contribution of meteorological changes to the observed concentration reductions of other species depends on the exact location. Based on OMI observations, Zhang, Z. et al. (2020) observed reductions in East Asia of about 33% and 41% for NO_2 and SO_2, respectively.

469   City-scale impacts of lockdown on NO$_2$ tropospheric column amounts for Wuhan and Beijing are presented in Sect.
470   3. Here, we investigate whether a lockdown signature can be detected from space at the regional scale for other key
471   pollutants by focusing on TROPOMI tropospheric column measurement of SO$_2$, CO, HCHO, and CHOCHO. We also
472   compare the identified changes with the marked changes in NO$_2$ concentration. Figure 5 compares monthly mean
473   tropospheric columns of those different species for February 2019 and 2020. The NO$_2$ and SO$_2$ tropospheric column
474   amounts are clearly lower in February 2020 compared to 2019. A small general reduction is also visible in the CO,
475   HCHO and glyoxal column amounts. As discussed before, many factors other than the lockdown measures may
476   explain changes in pollutant concentrations, such as the meteorology or emission reduction related to the timing of
477   holidays. Another difficulty to compare different years is the data sampling. In February 2019, large parts of Southern
478   China were covered by clouds, preventing space-based observation of the lowermost atmospheric layers. This is
479   clearly illustrated in the upper panel of Figure 5 showing CHOCHO column amounts, where data is missing over large
480   regions since this product uses the most stringent cloud filtering as compared to the other trace gases. Therefore, the
481   following detailed discussion only focuses on the northern part of China (black box in Figure 5 top left panel), even
482   though the lockdown measures were stricter in the region of Wuhan.

483

484

485
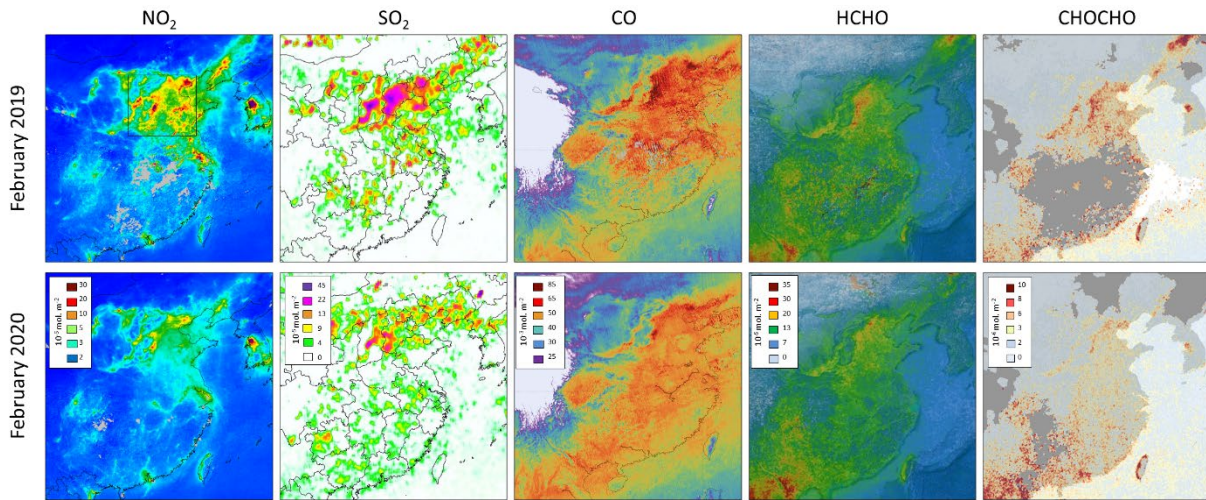
487   **Figure 5: Tropospheric and total columns for various trace gases over China as observed by TROPOMI over China in**
488   **February 2019 (upper panels) and 2020 (lower panels) in units of mol m^{-2}. The black box indicates the geographical region**
489   **used in the time series analysis (Figure 6). Note: the grey-shaded regions in NO$_2$ and CHOCHO panels (far left and far**
490   **right, respectively) indicate areas with little or no data available due to persistent local cloud cover.**

491

492   Figure 6 shows the seasonal cycles for tropospheric column amounts of TROPOMI NO$_2$, SO$_2$, CO, HCHO, and
493   CHOCHO for different years in northern China (region in black box highlighted in Figure 5) starting at the beginning
494   of the operational phase of the S5P/TROPOMI mission (30 April 2018). The different colored curves show two-week
495   medians of the daily mean tropospheric columns. In order to focus on the effect of COVID-19 lockdown measures for
496   HCHO and CHOCHO, the TROPOMI-based time series are compared with an OMI-based climatology for these

species using OMI data from 2010 to 2018, and shown by the black dashed curves. The associated uncertainties represent the interannual variability as estimated from OMI. This type of climatological reference based on a longer time series is not available for CO. Therefore, Figure 6 shows CO columns starting from 1 January 2018, which have been added to extend the time series even though the data sampling was more limited in the early phase of the mission. The light vertical boxes in January and February indicate the period of Chinese New Year holidays. Note that the 2020 holiday period was slightly extended as a first measure against the COVID-19 spread.
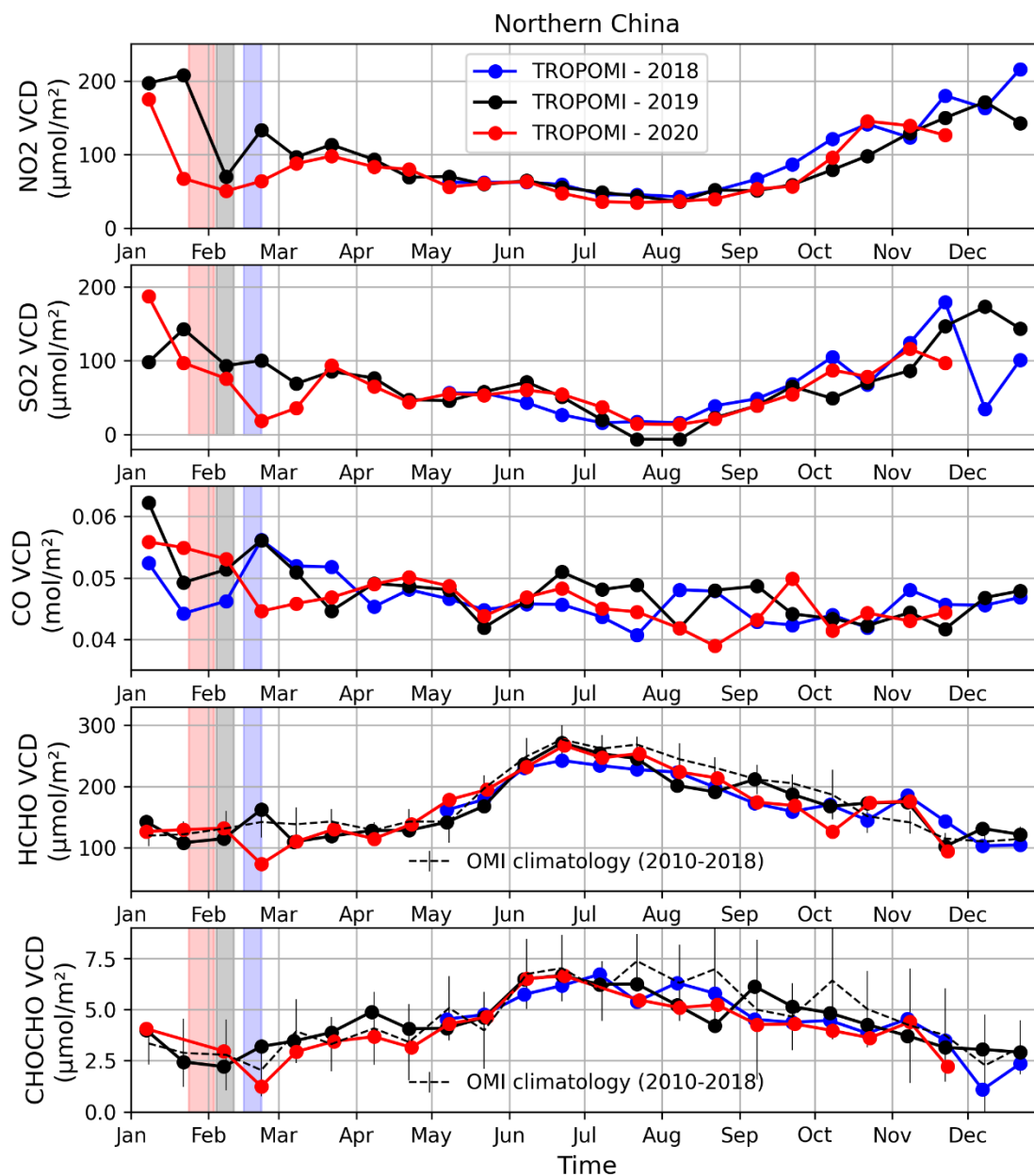
 Figure 6: Two-week median tropospheric column amounts of NO_2, SO_2, CO, HCHO and CHOCHO (from top to bottom)
for northern China (34°N-40°N; 110°E-120°E) in units of (micro)mol m^{-2}. The year 2020 is represented in red (2018 in blue,
2019 in black) and as indicated in the legend. The colored boxes correspond to the yearly Chinese New Year holidays for
those same years. The dashed black lines in the HCHO and CHOCHO panels represent a climatological seasonality as
obtained using the OMI data sets from 2010 to 2018 and the error bars represent the interannual variability (1-sigma
standard deviation).

Superimposed on the overall seasonal cycle of NO_2 (maximum during wintertime caused by a longer atmospheric lifetime), a clear reduction of the NO_2 columns is systematically observed which corresponds to the New Year festivities. While a quick return to higher values is usually observed after that period (Tan et al., 2009), the NO_2 columns remained lower for several weeks in 2020 likely as a consequence of the reduced traffic and industrial activities. For example, NO_2 column amounts at the end of February were about 45% lower than those of 2019. In March 2020, NO_2 columns return progressively to a similar level as compared to other years.

SO_2 emissions in China mostly originate from fossil fuel burning of coal and oil (Wang et al., 2018). Although Chinese SO_2 emissions have dropped significantly in the last decade (van der A et al., 2017; Zheng et al., 2018a), enhanced SO_2 columns are still observed in some regions of northern China (Figure 5). As illustrated in Figure 6, SO_2 column amounts are larger during wintertime mostly due to its longer atmospheric lifetime (Lee et al., 2011). No clear reduction could be related to the yearly holidays. However, in 2020 a sharp drop is observed starting in late January through mid-March with a reduction of up to 77% as compared to 2019. By late-March/early-April values returned to levels similar to previous years, which is consistent with the NO_2 lockdown signature.

In northern China the residential sector, consisting of mostly of emissions from heating and cooking, accounts for nearly half of the anthropogenic CO emissions, while the rest is distributed between traffic, power generation, and industry (Zheng et al., 2018b). Since the impact of lockdown measures is more limited for the residential sector as compared to the transport or industrial sectors, the response of CO to the lockdown measures is expected to be less distinct. Also, due to the longer atmospheric lifetime of CO (weeks to a month), the observed column amounts result from the accumulation of the trace gas over source regions and from long-range transport from regional and global sources. As such, meteorology significantly influences CO concentrations. The observed day-to-day variability is indeed large, leading to more scatter in the two-week median time series shown in Figure 6. The CO columns observed in late February/early March are lower than those observed in the last two years, which might be partly caused by the lockdown measures. However, the high temporal and spatial natural variability of the CO column amount is of the same magnitude as the possible COVID-19 lockdown signal, and the large, year-to-year interannual differences prevent firm conclusions from being drawn. Dedicated model simulations or a longer time series of the TROPOMI CO data may help to disentangle these effects in the future.

There are difficulties associated with the investigation of a possible lockdown signature in the satellite HCHO and CHOCHO data sets. Large uncertainties are associated with both of these column retrievals owing to their low optical depth. Moreover, HCHO and CHOCHO columns are dominated by biogenic emissions, which explains the observed seasonal pattern of HCHO and CHOCHO column values with a maximum during summertime as illustrated in Figure 6. Variability in meteorology (temperature changes, winds, precipitation) may lead to changes in column amounts on the same order of magnitude as the expected lockdown-related reduction in anthropogenic emission changes. The

546 interannual variability as inferred from the OMI data sets is estimated to be in the range of $1x10^{14}$ molec cm^{-2} (~30%)
547 and $1.2x10^{15}$ molec cm^{-2} (~12%) for CHOCHO and HCHO, respectively. Despite those issues, a clear minimum is
548 visible for both HCHO and CHOCHO in late February 2020, with columns significantly lower than 2019 and lower
549 than the OMI climatology (about -40% and -50% for HCHO and CHOCHO, respectively). The differences are also
550 larger than what can be explained by the typical interannual variability. This is in agreement with Sun et al. (2021),
551 who finds a significant HCHO decrease in the Northern China Plain. For glyoxal, a reduction of the column amounts
552 starts already in late January but similar reductions are observed in other years and might be related to a holiday effect
553 similar to that observed for NO$_2$.

554   It is interesting to note that local minima are observed simultaneously in late February 2020 for all species except
555 NO$_2$, despite the data products being generated using independent retrieval algorithms. This gives confidence into the
556 detected reductions and their anthropogenic origin. The small delay between the initial decrease in NO$_2$ column
557 amount and the observed decreases in the other trace gases is related to a combination of longer atmospheric lifetimes
558 and production being dominated by secondary processes as compared to NO$_2$ (Stavrakou et al., 2021) and is also likely
559 tied to the early timing of the Chinese New Year in 2020.

560 **5   Regional Observations for India**

561 India implemented strict national lockdown measures limiting activities across the country starting 24 March 2020 for
562 a period of 21 days in order to tackle the spread of the SARS-CoV-2 virus amongst its 1.3 billion inhabitants. The
563 initial stringent phase 1 restrictions were followed by careful region-based relaxations in three subsequent phases
564 carried out through the end of May as shown in Table 2.

565

566 **Table 2: Lockdown phases in India.**

	Dates	Measures	Reference
Phase 1	24 Mar to 14 Apr	Nearly all services and factories suspended.	Singh et al. (2020)
Phase 2	15 Apr to 3 May	Extension of lockdown with relaxations, reopening of agricultural businesses and small shops at half capacity.	BBC News (2020)
Phase 3	4 May to 17 May	Country split in 3 zones: (i) lockdown zone, (ii) zone with movement with private and hired vehicles, and (iii) normal movement zone.	India today (2020)
Phase 4	17 May to 31 May	Additional relaxations, more authority given to local bodies.	The Economic Times, 2020

567

568

569   Figure 7 gives an overview of TROPOMI observations of NO_2, SO_2, CO, HCHO, and CHOCHO, over India for

570   April 2020, thus covering most of phase 1 and 2 of the Indian lockdown, as compared to the same month in 2019. For

571   NO_2 and SO_2 the column amounts are clearly lower across the country in 2020 as compared to 2019. Although less

572   prominent, column amounts of CO, HCHO, and CHOCHO appear to be lower in April 2020 over the domain of the

573   Indo-Gangetic Plain (IGP), which is one of the most densely populated areas of the world with roughly 900 million

574   people.

575

576

577
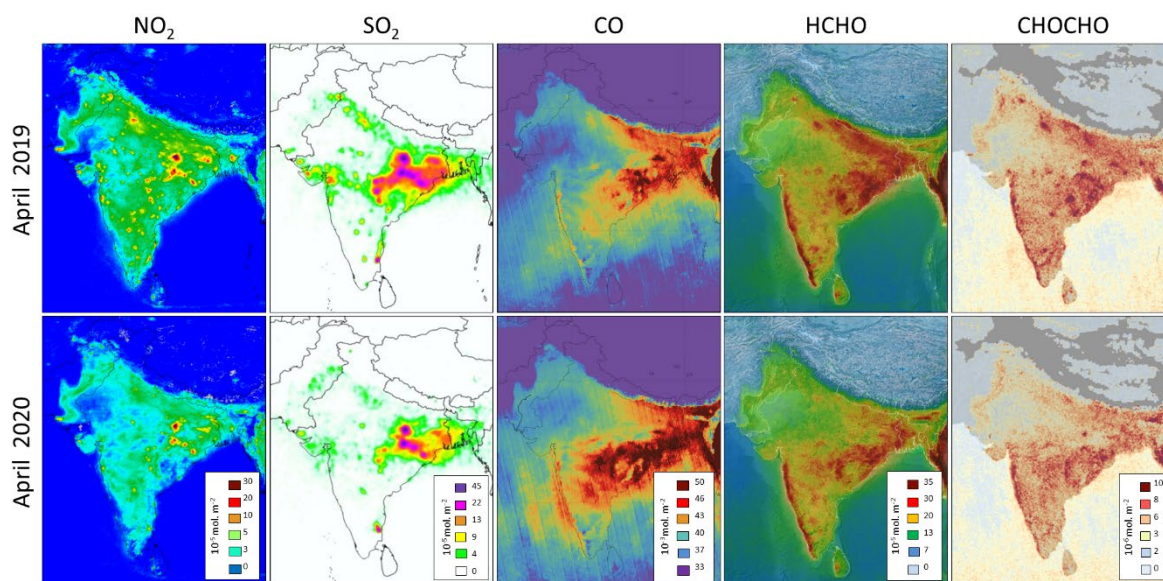
579   **Figure 7: Tropospheric and total columns maps for April 2019 (top row) and April 2020 (bottom row) for the various trace**
580   **gas species measured by TROPOMI from left to right, NO_2, SO_2, CO, HCHO and CHOCHO, shown in units of mol m^{-2}.**

581

582   The two main sources of NO_2 are road transport and power generation, each accounting for about 30% of total

583   anthropogenic emissions in India (Granier et al., 2019). During phase 1 of the lockdown the Tom-Tom traffic index

584   dropped by 80% (Aloi et al., 2020; Prabhjote, 2020) and energy consumption dropped by 25% compared to 2019

585   (Dattakiran, 2020; POSOCO, 2021) (Fig. D1). As such, we expect a strong reduction in NO_2 particularly in urban

586   areas due to large decreases in transport sector activities and we expect a weaker reduction near power plants due to

587   smaller decreases in energy demand.

588   Indeed, as indicated by the maps of NO_2 column amounts in Figure 7, a notable reduction in NO_2 can be seen in

589   April 2020 as compared to April 2019. A clear reduction is observed over major cities as well as over the eastern part

590   of India where most large power plants are located. Figure 8a shows the average NO_2 total column amounts as

591   measured by TROPOMI for 2018, 2019 and 2020, for the 40 largest cities in India selected on the basis of the number

592   of inhabitants (www.geonames.org) where NO_2 is averaged over a 15 x 15 km^2 area around each city center. When

593   both city centers and power plants are located within a 45 x 45 km^2 box, this box is excluded from the averages to

594   avoid potential outflow of one source to the other. A sharp reduction of 42% can be seen in the amount of NO$_2$ over

595   cities during the first phase of the lockdown period starting at the end of March, as compared to the same period in

596   2019. This initial drop in NO$_2$ is then followed by a slow but gradual increase in line with the successive relaxation

597   phases (Table 2). Power generation is a major source for NO$_2$ in India, in particular from coal-fired power plants.

598   When examining the average amount of NO$_2$ over the 100 largest coal-fired power plants (www.wri.org), we observe

599   a significant drop in NO$_2$ during phase 1 of the lockdown period. This drop, observed over coal-fired power plants of

600   23% as compared to 2019 (Figure 8b), is less pronounced than the observed drop in NO$_2$ over cities (Figure 8a). The

601   TROPOMI-observed reduction in NO$_2$ over coal-power plants is in line with the initial 25% decrease in maximum

602   electricity demand reported by National Load Dispatch Centre (NLDC) during phase 1 and tapering to an 8% decrease

603   during phase 4 of the lockdown as compared to 2019 (Fig. D1, Dattakiran, 2020).

604

605
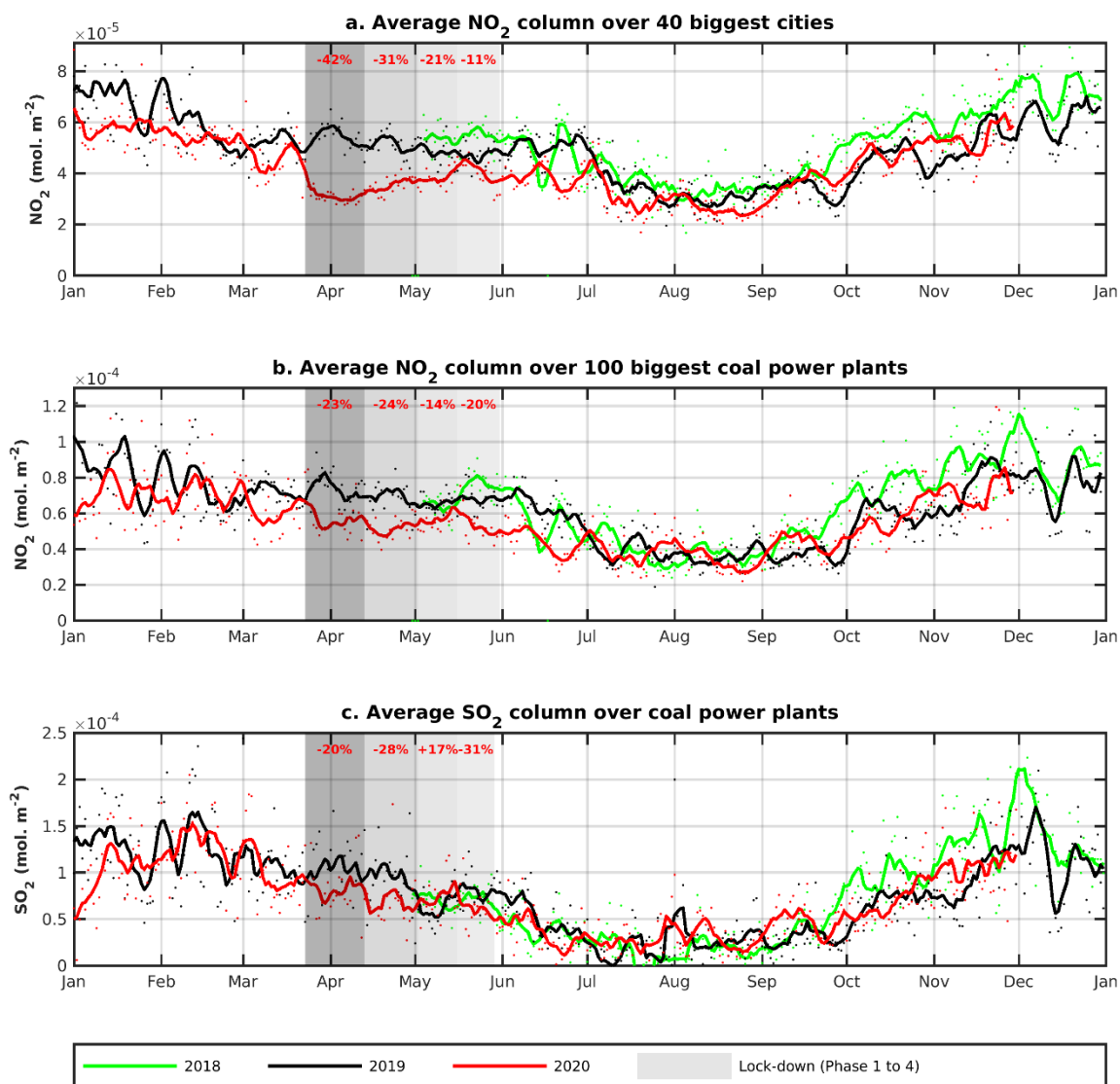
Figure 8: Average tropospheric NO₂ column amounts for May 2018 (green), 2019 (black) up until December 2020 (red) over the 40 largest Indian cities (top); over the 100 largest power plants in India (middle); and average SO₂ concentrations over the 59 largest SO₂-emitting power plants in India (bottom). The four different phases of the lockdown period are denoted by the different grey shading. For each phase, the reductions in NO₂ (or SO₂) concentrations are given relative to the same period in 2019. The dots are the daily means, and the solid lines represent the 7-day running means.

According to the CAMS-GLOB-ANT emission inventory for 2019 the major sources for SO_2 in India are power generation (65%) and industry (25%) (Granier et al., 2019). Since India largely relies on coal for producing energy, it is the world's top emitter of anthropogenic SO_2 (Li et al., 2017). So, most of the SO_2 signal we see in TROPOMI data for this region (Figure 7) is from coal-fired power plants, where contributions from oil and gas plants in India comprise a much smaller part of the signal (Fioletov et al., 2016). From Figure 7, a reduction in SO_2 is visible over most areas, and is especially noticeable for the easternmost part of India, which is India's largest SO_2-emitting region with more than 20 coal-fired power plants.

620   We have investigated the SO_2 VCD amounts over the largest power plants, and adapted the selection method used
621   for NO_2 by considering a larger area of 50 x 50 km² around each power plant. This is justified by (1) the longer lifetime
622   of SO_2 compared to NO_2, (2) the lower contamination by other sources, and (3) the need to reduce the noise on the
623   SO_2 data to more clearly isolate the signal from the power plant. The results of the averaged SO_2 VCD time series are
624   presented in Figure 8c. It should be noted that, compared to NO_2, an additional selection of the power plants was
625   applied. Based on the SO_2 VCD map for April 2019 (Figure 7), only the power plants with mean SO_2 columns larger
626   than 0.15 DU were considered (59 power plants in total). Although the signal is relatively weak for SO_2, we find very
627   similar reductions in SO_2 as compared to NO_2. Especially during the first two phases of the lockdown, a reduction of
628   about 20% is found which is in line with the NO_2 observations and the reported reduction in energy demand. In May,
629   for the different years, the consistency between NO_2 and SO_2 VCDs is less straightforward and the reason for this is
630   not fully understood. It should however be noted that the NO_2 and SO_2 data products do not use the same cloud
631   products for filtering and this might be a reason for discrepancy. Moreover, the possibility of a systematic
632   contamination of the NO_2 signal over power plants by other sources cannot be ruled out completely. A noticeable
633   feature of Figure 8b and Figure 8c is the overall excellent correspondence between NO_2 and SO_2 VCD evolution (on
634   short-term/seasonal basis, and outside the lockdown periods) as well as from year to year. This further strengthens the
635   observed COVID-19 related drop in both trace gases, although it is clear that meteorology and chemistry likely play
636   a large role in the observed VCD variability. Also, ground-based studies in New Delhi find a more important reduction
637   in NO_2 compared to SO_2 (Mahato et al., 2020; Kumari and Toshniwal, 2020).

638   For HCHO, CHOCHO, and CO, various regions over India have been investigated to detect a possible signal
639   resulting from COVID-19 lockdown measures. We could only identify such a signal in the densely populated areas of
640   the Indo-Gangetic Plain and New Delhi. These areas, due to the high intensity of traffic and industrial activities, are
641   most likely to exhibit large impacts on atmospheric pollution levels due to COVID-19 lockdown measures.

642   Figure 9 shows two-week averaged column values for HCHO, CHOCHO, and CO over the IGP and New Delhi,
643   based on TROPOMI data from January 2018 to June 2020. To support the interpretation of the observed seasonal and
644   interannual variations, Fig. D2 presents the corresponding temperature, precipitation amount, and fire count. The
645   temperature starts increasing in January and reaches a maximum in June. The period from July to September
646   corresponds to the monsoon season with heavy rains and lower temperatures, and therefore lower pollution levels.
647   Fire activity peaks around May with a second peak is observed in November for the IGP. The time series of the HCHO,
648   CHOCHO, and CO columns correlate with these seasonal events, although with a different amplitude. For example,
649   HCHO shows the strongest correlation with temperature (see Sect. 2.5), while CHOCHO mainly follows fire
650   emissions. The smaller amplitude in CO variations is caused by its longer lifetime.

651
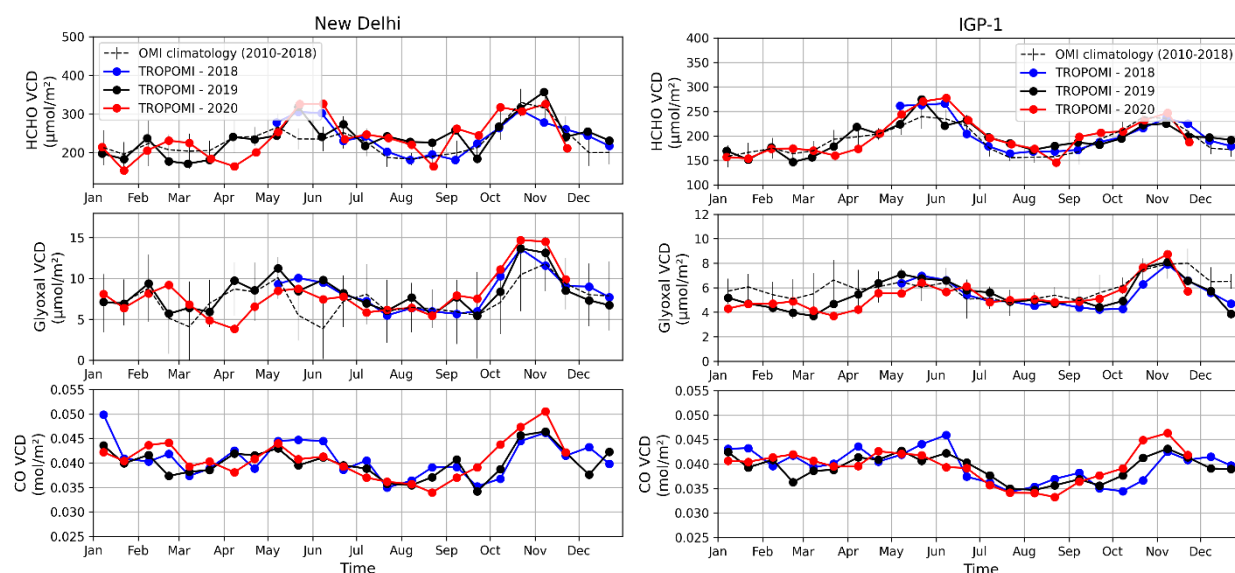
Figure 9: Time evolution of HCHO, CHOCHO, and CO over the densely populated Indo-Gangetic plain (right panel, defined by the region within this 4 coordinates: 29.5°N 72°E, 21.5°N 86°E, 24.5°N 88.5°E , 32.5°N 74.5°E), and over the megacity New Delhi (left panel, radius of 25 km, or 50 km for CHOCHO) as observed with TROPOMI. The year 2020 is represented in red (2018 in blue, 2019 in black). With the HCHO and CHOCHO time series, the OMI climatology is shown for comparison (dashed black line, 2010-2018), the error bars represent the interannual variability of the two-week averaged columns. The HCHO columns have been corrected in order to assume the same temperature every year (see Sect. 2).

659

660   A large part of the observed HCHO and CHOCHO columns for India are due to natural emissions which can vary

661   significantly due to changes in meteorology, in particular temperature and precipitation. Hence a possible reduction

662   of the anthropogenic VOC emissions due to the lockdown measures is expected to have a small contribution to the

663   variability of the measured columns. During the most stringent phase 1 lockdown, a reduction in HCHO column

664   amount is observed for the IGP and is even more pronounced over New Delhi (Figure 9 top panels; respectively -2

665   and -4x10^{15} molec cm^{-2} [-20% and -40%] compared to the OMI climatology for 2010-2018). In both cases, the

666   anomaly is larger than the interannual variations observed during this period (about 1.5x10^{15} molec cm^{-2}), where

667   changes in temperature or precipitation do not seem to explain the observed column decrease during phase 1. The

668   observed column decline is even more pronounced over New Delhi than over the IGP, suggesting that the origin of

669   the reduction is mostly anthropogenic.

670   The case for lockdown-driven reductions is further supported by the CHOCHO observations, which exhibit the

671   clearest COVID-19 signal during phase 1 of the lockdown (Figure 9). The reduction of CHOCHO during the lockdown

672   period over the IGP is slightly larger than the interannual variability of 1x10^{14} molec cm^{-2} (or -25%) as determined

673   from the OMI CHOCHO climatology. Similar to HCHO, the reduction in CHOCHO over New Delhi is twice as large

674   (-50%) and well beyond the 1-sigma OMI climatology range. Phase 2 is also characterized by lower CHOCHO column

675   amounts in 2020 as compared to 2019, but temperatures are also lower, unlike phase 1. Accounting for temperature-

676   driven variability (Sect. 2.5) brings the HCHO columns close to the mean HCHO seasonal levels. The somewhat more

677   pronounced effect of the lockdown on CHOCHO compared to HCHO in New Delhi is most likely due to the strong

678   contribution of anthropogenic VOC precursors to CHOCHO amounts (Chan Miller et al., 2016). Interestingly, fire

679   counts show that there were fewer fires in May 2020 compared to previous years (Fig. D2), most likely as a

680   consequence of the lockdown measures, which may also contribute to the lower glyoxal columns.

681   As it was the case for China, it is more difficult to identify a signal in CO column data driven by the COVID-19

682   lockdowns over India. An important reason for this is the much longer atmospheric residence time of CO that varies

683   depending on the OH concentration (Holloway et al., 2000). Moreover, according to bottom-up inventories, the major

684   anthropogenic CO source in India are due to the residential sector (42%), road transportation (21%), agricultural waste

685   burning (18%) and the industrial sector (16%) (Granier et al., 2019). Hence, during a lockdown we expect that the

686   main source of CO, residential, to be less affected. Figure 7 shows that the CO amounts in southern India are higher

687   in 2020 as compared to 2019. The enhanced CO values in 2019 and 2020 are detected above regions (e.g. Madhya

688   Pradesh, Odisha, and Chhattisgarh) where seasonal forest fires commonly occur in April/May (Chandra and Kumar

689   Bhardwaj, 2015, Srikanta et al. 2020). Thus, the enhancement of CO for the different years depends not only on the

690   fire activity but also on how the meteorological situation prevents or permits the accumulation of CO in the

691   atmosphere. To more fully address the reasons why CO is higher in 2020 than 2019, future studies could carry out

692   calculations using a chemical transport model. The long atmospheric residence time of CO complicates the

693   identification of COVID-19 lockdown signals. Also for CO we derived the full TROPOMI time series for the IGP and

694   New Delhi as shown in Figure 9 (lower panel). The time series for New Delhi in mid-April shows somewhat lower

695   CO values in 2020 compared to 2019, but the large natural variability of CO prevents clear identification of a COVID-

696   19 lockdown driven effect. In future, analysis of a longer TROPOMI CO time series or model experiments may help

697   to quantify the COVID-19 effects.

698

699   **6   Conclusions**

700   In this paper, we have analyzed the impact of COVID-19 lockdown measures on air quality around the globe, based

701   on observations of several trace gases from the Sentinel-5P/TROPOMI instrument. TROPOMI provides daily, global

702   observations of multiple trace gases, where the measured vertical column amounts are driven by emissions as well as

703   atmospheric and chemical processes of transport, transformation, and deposition. We compared the 2020 TROPOMI

704   data with similar periods from previous years and carried out additional analysis to disentangle changes in emissions

705   due to COVID-19 lockdown measures from meteorological variability, seasonal variability, and from other non-

706   lockdown emission drivers. We analyzed time series of NO_2 measurements from city to regional scales for several

707   locations around the globe, showing the potential of TROPOMI to globally monitor local to regional impacts of

708   COVID-19 lockdown measures on air quality and anthropogenic emissions. Furthermore, for the first time, we used

709   a combination of five trace gases observed by TROPOMI, specifically NO_2, SO_2, CO, HCHO and CHOCHO, to assess

710   the impact of COVID-19 related lockdown measures on trace gas concentrations.

711   From the global to city scale, we have illustrated consistent, sharp decreases in NO_2 column amount driven by the

712   COVID-19-related lockdown measures. These findings are based on detailed analysis of the distribution of NO_2 using

713   daily measurements from TROPOMI. For the city of Wuhan in China, the first city to issue a lockdown, NO_2

concentrations measured by TROPOMI were about 60% lower than the same period in February-March 2019. After China, lockdowns were issued across all continents and for the majority of countries from March through May 2020. For megacities all over the world, reductions in column amounts of tropospheric NO_2 range between 14% and 63%. The strength of the reduction depends on the type and efficiency of local measures carried out and on the relative contribution of traffic, industry, and power generation to NO_2 emissions for a given area. Owing to the unprecedented resolution of TROPOMI of about 5 km, reductions of different source contributions to NO_2 such as city traffic, highways (Liu et al., 2020), power plants (Miyazaki et al., 2020), industry, and shipping (Ding et al., 2020) can be estimated separately.

As demonstrated by time series analysis of the NO_2 observations, there is substantial variability even in two-week averages, which is attributable to meteorological variability. On average, we estimate the standard deviation of this variability to be about 13% (1-sigma standard deviation) for major cities in Europe, but locally the effect can sometimes be larger. The large and systematic reductions (30-60%) observed, however, cannot be explained by meteorological variability alone and are therefore attributed to the effect of the lockdown measures.

For SO_2, we observe significant column reductions in China and India over coal-fired power plants, which are the primary sources of anthropogenic SO_2 in these areas. Over northeastern China in late February 2020, large reductions of SO_2 vertical column amounts were observed, as a result of lockdown measures, with a decrease up to 77% as compared to the same time period in 2019, which cannot be explained by interannual variability alone. An analysis of SO_2 vertical column amounts over the largest SO_2-emitting power plants in India, reveals a reduction in SO_2 of about 25% during the first two phases of the lockdown, as compared to 2019. For India, the reductions in SO_2 were highly correlated with NO_2 reductions for the same power plants and with the national energy demand for that period.

The natural variability of HCHO and CHOCHO does not allow detection of a significant decrease due to the COVID-19 measures in most regions of the world based on TROPOMI observations alone. Exceptions are northern China and New Delhi, where observed reductions could be attributed to the lockdown measures. For northeastern China, a 50% reduction in the CHOCHO column amount is observed during the second half February, which is larger than the typical observed interannual variability of 30%. For HCHO, after correcting for the effect of seasonal and temperature variations, we observe a coincident 40% reduction. We analyzed column amounts of CO, CHOCHO, and HCHO over the Indo-Gangetic Plain, which is the most densely populated region of India. For CHOCHO and HCHO, we observed small reductions in column amount due the COVID-19 measures, where these observed effects are slightly larger than the interannual variability as determined using an OMI climatology (2010-2018). The observed reduction of 25% of CHOCHO in this region is of the same order as the typical interannual variability. A stronger reduction of 60% is observed for the city of New Delhi, which is similar to the reduction observed over northern China but occurs later due to the difference in lockdown timing. For HCHO, we also observe a significant 40% decrease over New Delhi in April, while over the whole Indo-Gangetic Plain, a decrease of 20% is observed.

For CO, reductions related to COVID-19 measures were much more difficult to identify, although over northern China we see that the reductions in CO correlate with those for HCHO and CHOCHO. We could not find a similar effect for CO over New Delhi. The fact that it is so hard to draw conclusions for CO based on the TROPOMI data alone is due to the high variability in CO driven by meteorological conditions, in combination with the difficulty of

distinguishing localized emission changes from the high and variable background values, caused by the long atmospheric lifetime of CO.

TROPOMI data have already been used in many publications (Gkatzelis et al., 2021; Bauwens et al., 2020; Liu et al., 2020; Huang et al., 2020) aiming to analyze the impact of COVID-19 lockdown measures on air pollution levels. Predominantly, these studies have been based on the use of TROPOMI NO_2 observations alone. We anticipate that the combined use of multiple trace gases from TROPOMI together with the high spatial resolution of the measurements, has large potential for a significantly improved sector-specific analysis of the impact of the COVID-19 lockdown measures than previously possible. Such a multi-species analysis offers promise for in-depth understanding of changes in air quality, the chemical interplay of pollutants in the atmosphere and their relation to emissions. While keeping in mind the importance of accounting for interannual, seasonal, and meteorologically driven variability (e.g. Miyazaki et al., 2020), it is clear that a detailed analysis cannot be based on TROPOMI observations alone. For more quantitative estimates of the impact of COVID-19 lockdown measures on trace gas concentrations and emissions, we need (inverse) models driven by high-quality meteorological analyses, or at least wind information or statistical relationships to account for weather-driven variability (Goldberg et al., 2020; Miyazaki et al., 2020; Ding et al., 2020).

In summary, our analyses using the most recent operational and scientific retrieval techniques have shown that by taking emission sources, atmospheric lifetime as well the seasonal and meteorological variability into account for a variety of trace gases measured by TROPOMI, rapid changes in anthropogenic emissions can be observed as induced by the implementation of regional COVID-19 lockdown measures. It is our hope that this case study will serve as reference for future analyses aimed at characterizing emission changes of not just NO_2, but for utilizing the concomitant observation of the variety of trace gases measured by TROPOMI.

Appendix A

Table A1: Summary of documentation available for TROPOMI operational data products from the Sentinel 5-P Library (https://sentinels.copernicus.eu/web/sentinel/technical-guides/sentinel-5p/products-algorithms).

Title	Document content description and product-specific reference	Document and Data links
Product Readme File (PRF)	Description of changes in product versions, recommended qa_values, and overall quality information	https://sentinels.copernicus.eu/web/sentinel/technical-guides/sentinel-5p/products-algorithms
NO₂	Eskes and Eichmann, 2020	qa_value recommendation: > 0.75
CO	Landgraf et al., 2020	qa_value recommendation: > 0.5
HCHO	De Smedt et al., 2020a	qa_value recommendation: > 0.5

Product User Manual (PUM)	Technical description of file formatting for each TROPOMI Level 2 operational data product	https://sentinels.copernicus.eu/web/sentinel/technical-guides/sentinel-5p/products-algorithms
NO₂	Eskes et al., 2020	
CO	Apituley et al., 2018	
HCHO	Romahn et al., 2020	
Algorithm Theoretical Basis Document (ATBD)	Detailed description of methods used for each TROPOMI L2 operational retrieval algorithm	https://sentinels.copernicus.eu/web/sentinel/technical-guides/sentinel-5p/products-algorithms
NO₂	van Geffen et al., 2019; 2021	Note: the 2019 ATBD describes v. 1.3.0 NO_2 data used in this paper.
CO	Landgraf et al., 2018	
HCHO	De Smedt et al., 2020b	
Quarterly Validation Report (ROCVR)	Detailed description of the latest validation available for each TROPOMI L2 operational dataset, product-specific	https://mpc-vdaf.tropomi.eu/
Operational Data Product Specifications	Product-specific overview pages with TROPOMI L2 dataset specifications, including how to access and how to cite each data product.	https://sentinels.copernicus.eu/web/sentinel/data-products
Operational Data Product Citation and Digital Object Identifier (DOI)	NO₂ Copernicus Sentinel 5-P, 2018a	doi:10.5270/S5P-s4ljg54
	CO Copernicus Sentinel 5-P, 2018b	doi:10.5270/S5P-1hkp7rp
	HCHO Copernicus Sentinel 5-P, 2018c	doi:10.5270/S5P-tjlxfd2

776

Appendix B

Appendix B contains additional information (Table B2) and description supporting the timing of COVID-19 driven emissions changes for global cities evaluated in this study and shown in Figure 2.

780

781   **Table B2. Details about the lockdown dates for the cities illustrated in Figure 2.**

City	Date (2020)	Comment	Reference
Wuhan	23 January	Lockdown Wuhan and Hubei province	Bloomberg (2020)
	8 April	Lockdown lifted	Bloomberg (2020)

Mumbai and New Delhi	24 March	Closure of schools, public transport and most businesses	BBC (2020a)
	31 May	Nationwide lockdown is extended until end of May	Aljazeera (2020a)
Manila	16 March	Philippines announced strict home quarantine	Calonzo and Jiao (2020)
	1 June	Most businesses allowed to re-open, but bars, restaurants and schools remain closed	Jennings (2020)
Madrid	14 March	Nationwide lockdown	Minder and Peltier (2020)
	9 May	Easing, stores and restaurants allowed to open	Goodman et al. (2020)
Milan	8 March	Locking down of Northern Italy including Milan	Horowitz (2020a)
	4 May	Loosening of strictest lockdown measures	Horowitz (2020b)
Paris	17 March	France imposes nationwide the restriction	Onishi and Méheut (2020)
	11 May	Gradually relaxed lockdown measures, most shops open	Makooi (2020)
Los Angeles	19 March	California enters lockdown	BBC (2020b)
	1 June	Reopening of some shops and restaurants	Patel (2020)
New York	22 March	New York state enters lockdown	BBC (2020b)
	13 June	Stay-at-home orders put in place until further notice	CBS News (2020)
Sydney	24 March	Strict lockdown measures adopted in Australia	Wahlquist (2020)
	15 May	New South Wales eases lockdown restrictions	Sonali (2020)
Auckland	23 March	In New Zealand stay-at-home orders are issued	Menon (2020)
	14 May	All businesses can open in New Zealand	Conforti (2020)
Mexico City	23 March	Most economic sectors stopped in Mexico	Pasley (2020)
	1 June	Gradual reopening of Mexico city	Associated Press (2020)
Lima	16 March	Stringent quarantine enforced by police and army	Collyns (2020)
	30 June	Peru extended nationwide lockdown through end of June	Aljazeera (2020b)
Sao Paulo	24 March	Start of lockdown, but measures were largely ignored	Uchoa (2020)

	31 May	Quarantine extended through May	CGTN (2020)
Buenos Aires	20 March	Argentina under mandatory lockdown	Do Rosario and Gillespie (2020)
	28 June	Lockdown extended	Misculin and Garrison (2020)
Baghdad	22 March	Iraq imposed a total nationwide lockdown	The Star (2020)
	21 April	Relaxed restrictions: shops reopen for limited hours	Saleh (2020)
	20 May	In Baghdad strict lockdown re-imposed for 6 districts	Saleh (2020)
Lagos	30 March	Stay-at-home order, markets open for limited hours	Orjinmo (2020)
	4 May	Easing of restrictions, but schools, bars, and cinemas remain closed	Mbah (2020)
Johannesburg	26 March	Stay-at-home orders issued in South Africa	Winter (2020)
	1 June	Most economic sectors permitted to operate	Aljazeera (2020c)

782

Detailed observations of NO_2 reductions in major cities worldwide

Three examples of lockdown-related NO_2 column reductions in major cities are shown for Santiago, Paris and New Delhi in Figure 1 with time windows selected to reflect region-specific lockdown periods. A strong reduction in the NO_2 tropospheric concentration of about 40% is observed over Santiago. In Paris, the NO_2 levels for the period 15 March to 15 April 2020 are about a factor of two lower than in March-April 2019 (see also Figure 4). For New Delhi the reduction is even more striking in comparison to April 2019 (about a factor of 3, Figure 2c). Both Paris and New Delhi also show significant reductions in background values around the cities. Background locations are subject to a variety of wind directions and sometimes downwind of city plumes thus influencing background concentrations. Such plumes are typically on the order of 100 km long, and, given the atmospheric residence time of NO_2 (2-12 hours), these plumes can fill the small domains around Paris and New Delhi shown in Figure 1.

In Wuhan, the first city to issue quarantines and lockdown measures, the observed NO_2 column drastically declined (-60%) between 23 January and 8 April 2020 compared to the same period in 2019 (Figure 2a, Table B2). This decrease is in good agreement with estimated reductions for the period 11 February to 2 March 2020 based on TROPOMI NO_2 (-43%, Bauwens et al., 2020) and in situ NO_2 observations in Wuhan (-55%, Shi and Brasseur, 2020). However, it should be noted that there was strong day-to-day variability in the NO_2 column amount due to meteorological factors, as well as missing data over Wuhan in February 2019 due to clouds. Model calculations by Liu et al. (2020) indicate that meteorological variability could have led to increased NO_2 columns in 2020 compared to 2019, suggesting that the observed NO_2 reductions underestimate the impact of emission reductions due to COVID-19. The partial lifting of the restrictions on 8 April led to a progressive increase in NO_2 levels, yet remained lower than in 2019, likely because the population was still advised to stay at home and schools remained closed. A similar response in NO_2 levels was observed in Beijing. The decreases were less pronounced (-40%) and are in excellent agreement with the

804   reported decrease based on in situ NO_2 measurements (-40%, Shi and Brasseur, 2020). The weaker response could be

805   due to the less drastic measures adopted in Beijing, because locally sustained COVID-19 cases were lower than in the

806   Hubei province (Leung et al., 2020). Strong NO_2 reductions were observed for other Chinese cities, like Nanjing,

807   Qingdao, and Zhengzhou, based on TROPOMI NO_2 observations (Bauwens et al., 2020).

808   India enforced strict restrictions of human activities on 24 March 2020 to tackle the spread of COVID-19. In New

809   Delhi and Mumbai, the onset of the lockdown induced a sharp decline in the observed NO_2 columns (by a factor of

810   2). The columns remained low during the entire lockdown period (-56% and -46%, respectively) (see Table 2 for

811   timing of Indian lockdown phases). This is very much in line with the decreases reported in New Delhi based on NO_2

812   data from monitoring stations, -53% (Mahato et al., 2020) and -48% (Jain and Sharma, 2020).

813   As compared to other cities, a very strong NO_2 decrease was observed in Lima (-63%), where strict regulations to

814   stay indoors were enforced (Collyns, 2020). A drastic drop in NO_2 compared to the 2019 levels marked the start of

815   the lockdown, and the levels remained very low throughout the entire lockdown period. The gradual increase of NO_2

816   columns in Lima and other Southern Hemispheric cities from January to May (Figure 2j) reflects the natural seasonal

817   variation when levels peak during the Southern Hemispheric winter, as temperatures decrease and NO_2 lifetime

818   increases.

819   In Buenos Aires, the observed reduction was not as strong compared to Lima for the entire lockdown period (-34%,

820   Table B2), but was particularly marked during the first month of the lockdown (20 March through 20 April 2020),

821   due to a compulsory quarantine period and strict limitation of activities for many sectors. Although partial lifting of

822   measures was issued after 10 April for many provinces in Argentina, the measures in the Buenos Aires agglomeration

823   were maintained due to the elevated number of cases (Raszewski and Garrison, 2020). More moderate reductions are

824   found for Mexico City (-22%) and Santiago (-23%) during the lockdown in comparison to the same period in 2019,

825   that could be attributed to less strict adherence to and enforcement of lockdown measures (Uchoa, 2020; Pasley, 2020).

826   Strong reductions were observed over the entire lockdown period in the heavily hit cities in southwest Europe, Los

827   Angeles, and New York, with reductions ranging between -32% and -54% (Bauwens et al., 2020). It should be noted

828   however, that in these regions, the start of the lockdown period is generally less marked partly because the lockdowns

829   were not as strictly enforced in Europe and the U.S. as in China and India. Moreover, the observed TROPOMI data

830   displays a strong variability attributable to meteorology, e.g. over Paris, New York and Los Angeles in 2019.

831   In Sydney, the reduction was moderate (-14%) and delayed with respect to the onset of the measures (Figure 2g).

832   This could be related to observations of less strict compliance in the early period of lockdown measures (New South

833   Wales Public Health, 2020). A rapid and strong decrease was observed for NO_2 column amount as a result of lockdown

834   measures in Auckland, New Zealand (-55%). Similarly, the lockdown measures in New Zealand were implemented

835   swiftly with high levels of compliance (Matthews, 2020). The end of the lockdown coincided with a strong increase

836   in NO_2 pollution, from 1.8×10^{15} molec cm^{-2} to 3×10^{15} molec cm^{-2} in the last three weeks of May.

837   In Africa, Nigeria is among the countries most affected by COVID-19 and reported the first confirmed case in sub-

838   Saharan Africa (Odunsi, 2020; Adigun and Anna, 2020). A two-week lockdown period was put in place for Lagos

839   starting 30 March. The NO_2 column amount decreased by 33% during the lockdown with respect to the same period

840   of 2019 and remained lower even after the lifting of restrictions on 4 May (Table B2). An NO_2 column decrease of

841   similar magnitude (-35%) was observed in Johannesburg (Figure 2p), where a national lockdown was issued on 26

842   March 2020, with a gradual easing of restrictions starting 1 May. In Sub-Saharan Africa, the emission reductions in

843   April were significant for larger populous and industrialized areas, whereas no noticeable drop was found in less

844   developed regions (Masaki et al., 2020).

845   Finally, the Iraqi capital of Baghdad faced an initial lockdown from 22 March through 21 April. A second partial

846   lockdown was issued starting 20 May in response to a sharp increase in COVID-19 cases due to the temporary

847   relaxation of restrictions to allow the celebration of Ramadan in late April (Table B2). The NO_2 column responded

848   quickly (Figure 2n) as confirmed by the rapid decrease once curfew measures were issues in late-May.

849   Figure 3 and Figure 4 illustrate the tropospheric column amount of NO_2 over Europe, focusing on Milan, Madrid,

850   Paris and Berlin, extending the analysis to 1 December. In France, Spain and Italy we detect strong reductions of NO_2,

851   which can be largely attributed to the lockdown measures. In Berlin, the measured differences are smaller, and a more

852   detailed analysis of the meteorological variability is needed to quantify the impact of the lockdown (see Figure 3).

853   The extended time series shows a recovery of the NO_2 pollution levels to pre-COVID-19 values. However, the

854   recovery is not complete, suggesting that remaining restrictions, new stay-at-home life and working practices, together

855   with a downturn in industrial and service-based activities have contributed to a longer lasting impact.

856   **Appendix C**

857   Appendix C contains figures which support the technical understanding of individual retrieval algorithms.

858
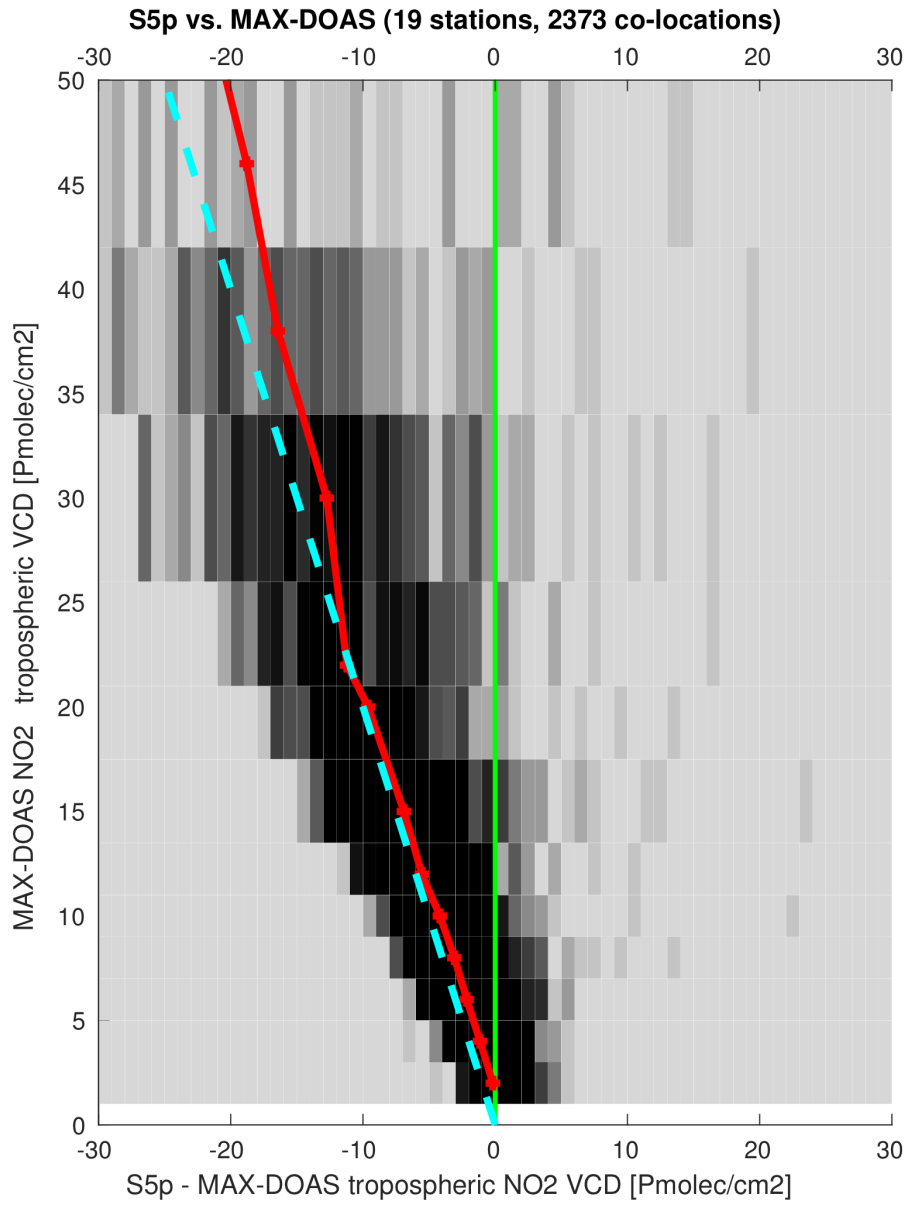
Figure C1: Bias in S5p-TROPOMI tropospheric NO₂ as estimated from comparisons to co-located ground-based MAX-DOAS measurements, presented as a function of the ground-based VCD measurement. The grey-scale background represents a 2-D histogram, where the median difference per MAX-DOAS VCD bin is shown as the red curve, and the blue dashed line shows a multiplicative bias (b) model with b ~ 0.5 x VCD. More details on the ground-based data and co-location scheme can be found in Verhoelst et al., 2021.

SO$_2$ vertical column (DU) - April 2019
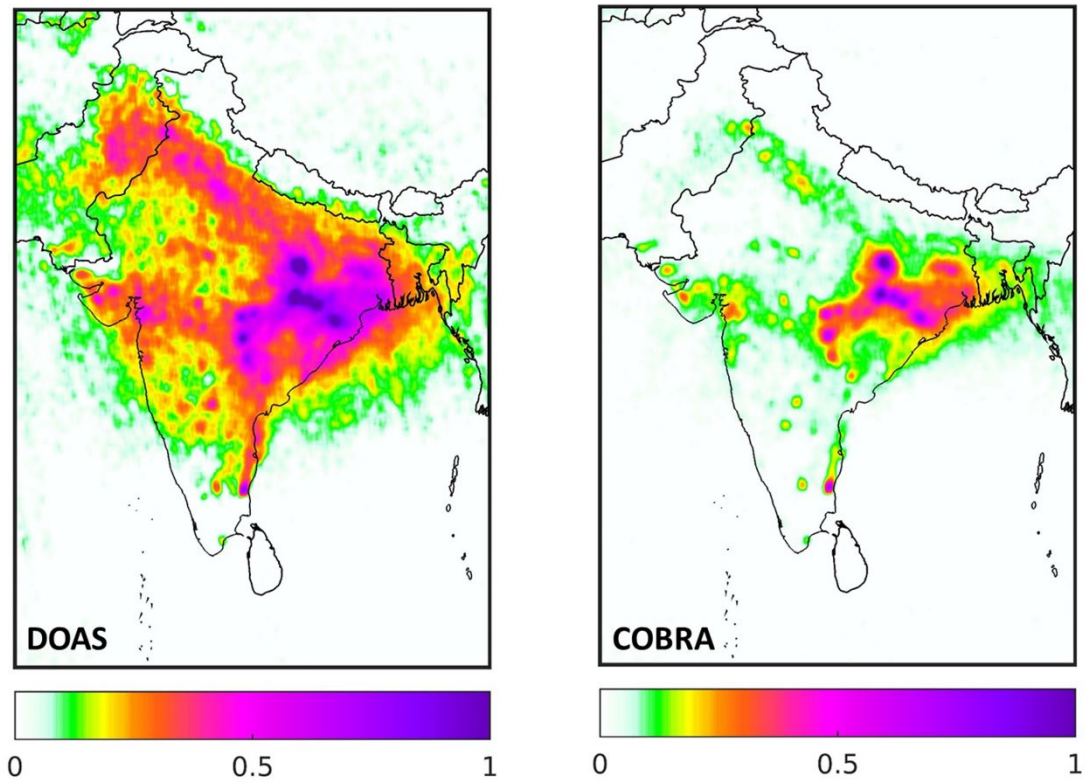
Figure C2: Monthly averaged TROPOMI SO$_2$ columns over India for April 2019, from (left) DOAS operational product and (right) COBRA scientific product. The reduction in noise and offsets as described and illustrated in Theys et al. (2021) can also be seen here where there is more contrast between the background and the individual point sources (power plants, darker pink and purple) can be better discerned in the COBRA SO$_2$ map.
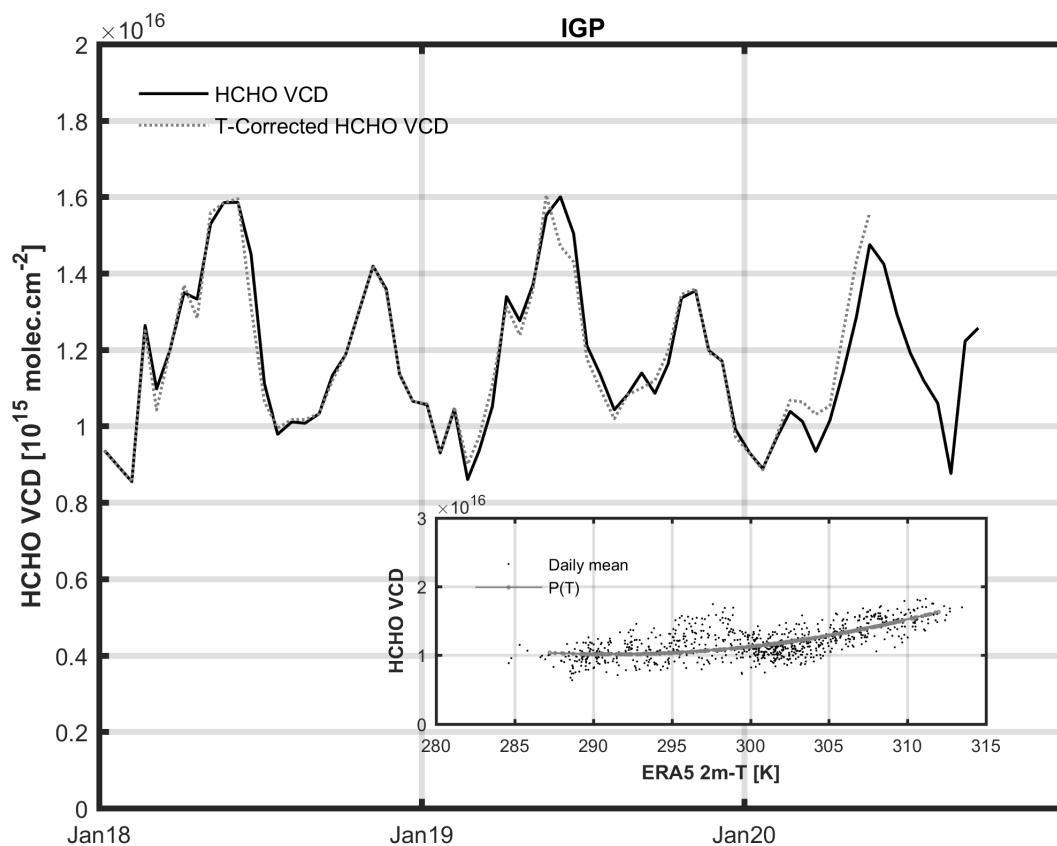
875 **Figure C3: Example of temperature correction of the TROPOMI HCHO tropospheric columns in the Indogangetic Plain**
876 **region. The dashed line presents the HCHO columns after correction using climatological temperatures. The correlation**
877 **between the local daily temperatures from ERA5-Land 2m and the HCHO columns is shown inset for the entire period.**

878 **Appendix D**

879 Appendix D contains additional figures that support the interpretation timing of observed changes in COVID-19
880 driven emissions related to power generation (Fig. D1) and meteorological conditions (Fig. D2).
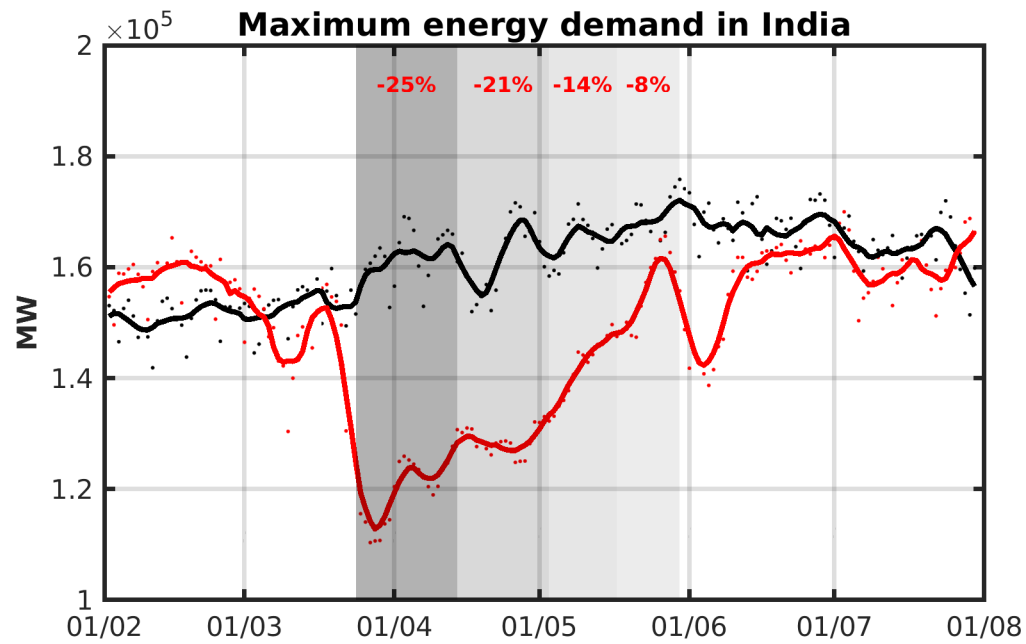
882   **Figure D1: Maximum energy demand over India during the period of the lockdown (red) compared to the same period in**
883   **2019 (black), For each of the phases of the lockdown the reductions in maximum energy demand is given relative to the**
884   **same period in 2019. Data from: www.posoco.in/covid-19.**

885

886

887

888

889

890

891

892

893

894
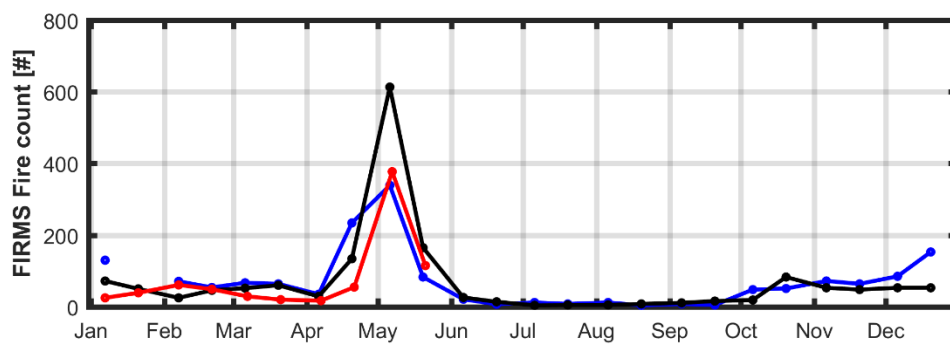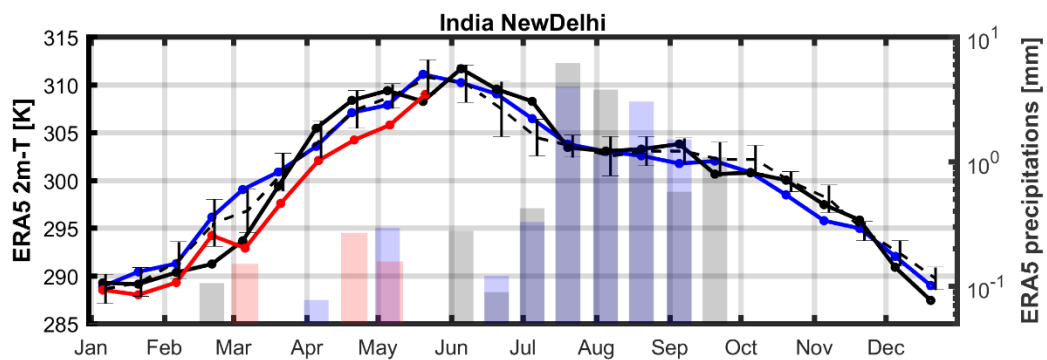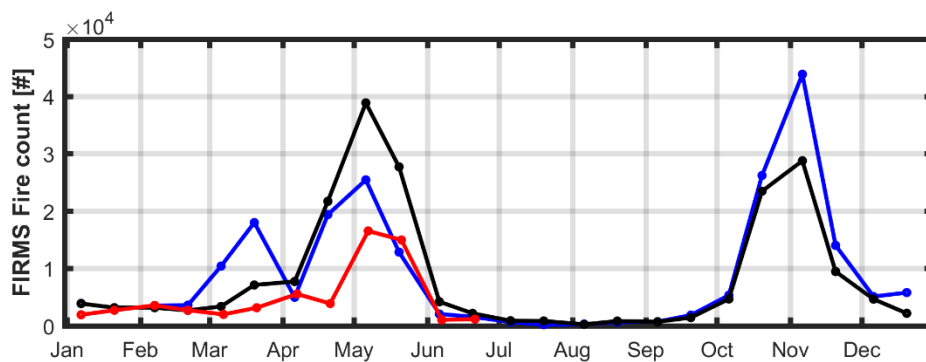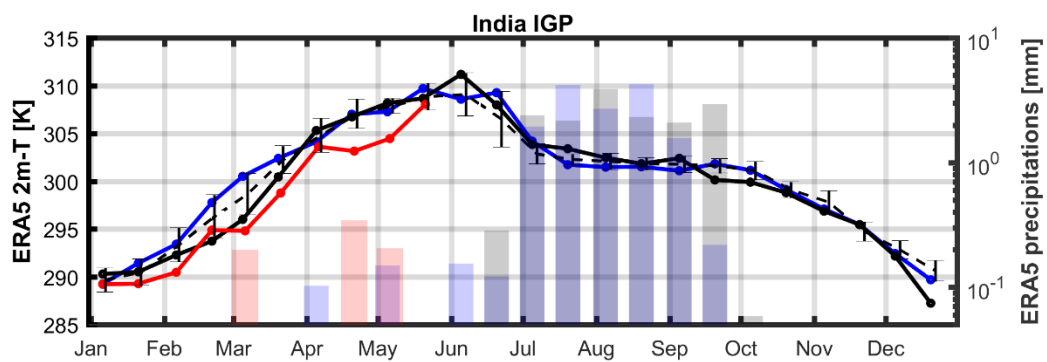
Figure D2: Meteorological and fire count information for the same regions as shown in Figure 9 (IGP plain upper two panels, and New Delhi lower two panels). Near-surface temperature and precipitation diagrams (top panel and second from bottom) show the two-week average temperature at 2m as lines and precipitation amounts as bars (source ERA5, Muñoz Sabater, 2019b). Second from top and bottom panels show fire counts (source FIRMS, https://earthdata.nasa.gov/firms). The year 2020 is represented in red, 2019 in black, and 2018 is in blue.

Data Availability

Operational versions of all Copernicus Sentinel 5-P Data TROPOMI data are freely available from the European Union/ESA/Copernicus Sentinel-5P Pre-Operations Data Hub (https://s5phub.copernicus.eu; S5P Pre-Ops Data Hub, 2021). The TROPOMI COBRA SO_2 dataset is available on request as described in Theys et al., 2021. OMI HCHO and NO_2 datasets are openly available on http://www.qa4ecv.eu/ecvs. TROPOMI Glyoxal data is available upon request as a part of the ESA S5p+I GLYRETRO project as detailed on the project website: https://glyretro.aeronomie.be/.

Author Contributions

PFL conceptualized, initiated, and managed this manuscript with contributions from IA, MB, TB, IDS, HE, CL, TS, DSZ, NT, MVR, PV, and TV. Formal analysis was carried out by MB, TB, IDS, HE, CL, and NT. DL and FR provided data curation and software support for TROPOMI HCHO data products. DSZ prepared, edited, and co-managed the manuscript with contributions from IA, MB, TB, IDS, HE, CL, PFL, TS, NT, MVR, PV, and TV.

Competing Interests

The authors declare that they have no conflict of interest.

Acknowledgements

We acknowledge financial support from the following projects: ESA S5P MPC (4000117151/16/I-LG); Netherlands Space Office TROPOMI Science Project; ESA S5p+Innovation GLYRETRO and ICOVAC projects (No. 4000127610/19/I-NS); Belgium Prodex TRACE-S5P (PEA 4000105598), and TROVA-2 (PEA 4000130630); Belgium BRAIN-2.be LEGO-BEL-AQ; EU FP7 QA4ECV project (grant no. 607405). This paper contains modified Copernicus data (2018/2020) processed by KNMI, BIRA-IASB, DLR, and SRON.

References

van der A, R., Mijling, B., Ding, J., Koukouli, M., Liu, F., Li, Q., Mao, H., and Theys, N.: Cleaning up the air: Effectiveness of air quality policy for SO_2 and NO_x emissions in China, Atmos. Chem. Phys., 17, 1775-1789, doi:10.5194/acp-17-1775-2017, 2017.

927

Adigun, B. and Anna, C.: Nigeria confirms 1st case of new virus in sub-Saharan Africa, AP News, https://apnews.com/article/5de56b2fcaffae583c7c57b82c1a4fff, last access: 30 March 2021, 2020.

Aljazeera: Coronavirus in India: What we know about world's largest lockdown, https://www.aljazeera.com/news/2020/05/india-coronavirus-crisis-200519120521747.html, last access: 17 June 2020, 2020a.

Aljazeera: Peru extends nationwide lockdown until end of June, https://www.aljazeera.com/news/2020/05/peru-extends-nationwide-lockdown-june-200523073017946.html, last access: 17 June 2020, 2020b.

Aljazeera: South Africa coronavirus lockdown to ease from June 1, https://www.aljazeera.com/news/2020/05/ramaphosa-south-africa-coronavirus-lockdown-ease-june-1-200525070634938.html, last access: 17 June 2020, 2020c.

Aloi, A., Alonso, B., Benavente, J., Cordera, R., Echániz, E., González, F., Ladisa, C., Lezama-Romanelli, R., López-Parra, Á., Mazzei, V., Perrucci, L., Prieto-Quintana, D., Rodríguez, A. and Sañudo, R.: Effects of the COVID-19 Lockdown on Urban Mobility: Empirical Evidence from the City of Santander (Spain), Sustainability, 12(9), 3870, doi:10.3390/su12093870, 2020.

Alvarado, L., Richter, A., and Lerot, C.: GLYoxal Retrievals from TROPOMI (GLYRETRO) Validation Report, S5p+Innovation – theme 1 (CHOCHO), 5p+I_CHOCHO_BIRA_VR, 1.1, 35 pp., https://glyretro.aeronomie.be/, 2020.

Apituley, A., Pedergnana, M., Sneep, M., Veefkind, J. P., Loyola, D., Landgraf, J., and Borsdorff, T.: Sentinel-5 precursor/TROPOMI Level 2 Product User Manual Carbon Monoxide, document number: SRON-S5P-LEV2-MA-002, 1.0.0, SRON Netherlands Institute for Space Research, Utrecht, The Netherlands, https://sentinels.copernicus.eu/web/sentinel/technical-guides/sentinel-5p/products-algorithms, 2018.

Associated Press: Mexico City will begin gradually reopening June 1, mayor says, https://www.latimes.com/world-nation/story/2020-05-21/mexico-city-will-begin-gradual-reopening-coronavirus-june-1, last access: 17 June 2020, 2020.

Baldasano, J. M.: COVID-19 lockdown effects on air quality by NO_2 in the cities of Barcelona and Madrid (Spain), Sci. Total Environ., 741, 140353, doi:10.1016/j.scitotenv.2020.140353, 2020.

962

963 Barré, J., Petetin, H., Colette, A., Guevara, M., Peuch, V.-H., Rouil, L., Engelen, R., Inness, A., Flemming, J., Pérez

964 García-Pando, C., Bowdalo, D., Meleux, F., Geels, C., Christensen, J. H., Gauss, M., Benedictow, A., Tsyro, S., Friese,

965 E., Struzewska, J., Kaminski, J. W., Douros, J., Timmermans, R., Robertson, L., Adani, M., Jorba, O., Joly, M., and

966 Kouznetsov, R.: Estimating lockdown-induced European NO_2 changes using satellite and surface observations and air

967 quality models, Atmos. Chem. Phys., 21, 7373–7394, doi:10.5194/acp-21-7373-2021, 2021.

968

969 Bauwens, M., Stavrakou, T., Müller, J.-F., De Smedt, I., Van Roozendael, M., van der Werf, G. R., Wiedinmyer, C.,

970 Kaiser, J. W., Sindelarova, K. and Guenther, A.: Nine years of global hydrocarbon emissions based on source inversion

971 of OMI formaldehyde observations, Atmos. Chem. Phys., 16(15), 10133–10158, doi:10.5194/acp-16-10133-2016,

972 2016.

973

974 Bauwens, M. Compernolle, S., Stavrakou, T., Müller, J.-F., van Gent, J., Eskes, H., Levelt, P. F., van der A, R.,

975 Veefkind, J. P., Vlietinck, J., Yu, H., and Zehner, C.: Impact of coronavirus outbreak on NO_2 pollution assessed using

976 TROPOMI and OMI observations, Geophys. Res. Lett., 47(11), doi:10.1029/2020GL087978, 2020.

977

978 BBC: India extends coronavirus lockdown by two weeks, https://www.bbc.com/news/world-asia-india-52698828, last

979 access: 17 June 2020, 2020a.

980

981 BBC: Earlier coronavirus lockdown 'could have saved 36,000 lives', https://www.bbc.com/news/world-us-canada-

982 52757150, last access: 17 June 2020, 2020b.

983

984 Beirle, S., Borger, C., Dörner, S., Li, A., Hu, Z., Liu, F., Wang, Y., and Wagner, T.: Pinpointing nitrogen oxide

985 emissions from space, Sci. Adv. 5, doi:10.1126/sciadv.aax9800, 2019.

986

987 Beirle, S., Borger, C., Dörner, S., Eskes, H., Kumar, V., de Laat, A., and Wagner, T.: Catalog of NOx emissions from

988 point sources as derived from the divergence of the NO2 flux for TROPOMI, Earth Syst. Sci. Data, 13, 2995–3012,

989 https://doi.org/10.5194/essd-13-2995-2021, 2021.

990

991 Bloomberg News: China to lift lockdown over virus epicenter Wuhan on April 8,

992 https://www.bloomberg.com/news/articles/2020-03-24/china-to-lift-lockdown-over-virus-epicenter-wuhan-on-april-

993 8, last access: 1 July 2020, 2020.

994

995 Boersma, K. F., Eskes, H. J., Richter, A., De Smedt, I., Lorente, A., Beirle, S., van Geffen, J. H. G. M., Zara, M.,

996 Peters, E., Van Roozendael, M., Wagner, T., Maasakkers, J. D., van der A, R. J., Nightingale, J., De Rudder, A., Irie,

997 H., Pinardi, G., Lambert, J.-C., and Compernolle, S.: Improving algorithms and uncertainty estimates for satellite NO_2

998 retrievals: Results from the Quality Assurance for Essential Climate Variables (QA4ECV) project, Atmos. Meas.

999 Tech., 11, 6651-6678, doi:10.5194/amt-11-6651-2018, 2018.

1000

Borsdorff, T., Hasekamp, O. P., Wassmann, A., and Landgraf, J.: Insights into Tikhonov regularization: Application to trace gas column retrieval and the efficient calculation of total column averaging kernels, Atmos. Meas. Tech., 7(2), 523–535, 2014.

Borsdorff, T., Tol, P., Williams, J. E., de Laat, J., aan de Brugh, J., Nédélec, P., Aben, I., and Landgraf, J.: Carbon monoxide total columns from SCIAMACHY 2.3 µm atmospheric reflectance measurements: towards a full-mission data product (2003–2012), Atmos. Meas. Tech., 9, 227–248, doi:10.5194/amt-9-227-2016, 2016.

Borsdorff, T., aan de Brugh, J., Hu, H., Nédélec, P., Aben, I., and Landgraf, J.: Carbon monoxide column retrieval for clear-sky and cloudy atmospheres: a full-mission data set from SCIAMACHY 2.3 µm reflectance measurements, Atmos. Meas. Tech., 10, 1769–1782, doi:10.5194/amt-10-1769-2017, 2017.

Borsdorff, T., aan de Brugh, J., Hu, H., Hasekamp, O., Sussmann, R., Rettinger, M., Hase, F., Gross, J., Schneider, M., Garcia, O., Stremme, W., Grutter, M., Feist, D. G., Arnold, S. G., De Mazière, M., Kumar Sha, M., Pollard, D. F., Kiel, M., Roehl, C., Wennberg, P. O., Toon, G. C., and Landgraf, J.: Mapping carbon monoxide pollution from space down to city scales with daily global coverage, Atmos. Meas. Tech., 11, 5507–5518, doi:10.5194/amt-11-5507-2018, 2018.

Borsdorff, T., aan de Brugh, J., Pandey, S., Hasekamp, O., Aben, I., Houweling, S., and Landgraf, J.: Carbon monoxide air pollution on sub-city scales and along arterial roads detected by the Tropospheric Monitoring Instrument, Atmos. Chem. Phys., 19, 3579–3588, doi:10.5194/acp-19-3579-2019, 2019.

Borsdorff, T., García Reynoso, A., Maldonado, G., Mar-Morales, B., Stremme, W., Grutter, M., and Landgraf, J.: Monitoring CO emissions of the metropolis Mexico City using TROPOMI CO observations, Atmos. Chem. Phys., 20, 15761–15774, doi:10.5194/acp-20-15761-2020, 2020.

Bovensmann, H., Burrows, J. P., Buchwitz, M., Frerick, J., Noel, S., Rozanov, V. V., Chance, L.V., and Goede, A.P.H.: SCIAMACHY: Mission objectives and measurement modes, Atmos. Sci., 56, 127-150, 1999.

Braaten, J.: Monitoring air quality with S5P TROPOMI data, Medium, https://medium.com/google-earth/monitoring-air-quality-with-s5p-tropomi-data-4f6b0aebe1c0, last access: 20 June 2021, 2020.

Broomandi, P., Karaca, F., Nikfal, A., Jahanbakhshi, A., Tamjidi, M., and Kim, J. R.: Impact of COVID-19 Event on the Air Quality in Iran. Aerosol Air Qual. Res., 20, 1793–1804, doi:10.4209/aaqr.2020.05.0205, 2020.

1035

1036   Calonzo, A. and Jiao C.: Duterte expands Philippine lockdown to 60 million people,
1037   https://www.bloomberg.com/news/articles/2020-03-16/duterte-widens-lockdown-to-main-philippine-island-to-fight-
1038   virus, last access: 17 June 2020, 2020a.

1039

1040   Cao, H., Fu, T.-M., Zhang, L., Henze, D. K., Miller, C. C., Lerot, C., Abad, G. G., De Smedt, I., Zhang, Q., van
1041   Roozendael, M., Hendrick, F., Chance, K., Li, J., Zheng, J. and Zhao, Y.: Adjoint inversion of Chinese non-methane
1042   volatile organic compound emissions using space-based observations of formaldehyde and glyoxal, Atmos. Chem.
1043   Phys., 18(20), 15017–15046, doi:10.5194/acp-18-15017-2018, 2018.

1044

1045   CBS News: Lockdown extended for most of coronavirus-battered New York, https://www.cbsnews.com/news/new-
1046   york-stay-at-home-extended-coronavirus-lockdown/, last access: 17 June 2020, 2020.

1047

1048   CGTN: Sao Paulo extends the quarantine through May, https://newsus.cgtn.com/news/2020-05-10/Sao-Paulo-
1049   extends-quarantine-through-May-QmDnOJo6bK/index.html, last access: 1 July 2020, 2020.

1050

1051   Chan Miller, C., Jacob, D. J., González Abad, G., and Chance, K.: Hotspot of glyoxal over the Pearl River delta seen
1052   from the OMI satellite instrument: implications for emissions of aromatic hydrocarbons, Atmos. Chem. Phys., 16,
1053   4631–4639, doi:10.5194/acp-16-4631-2016, 2016.

1054

1055   Chandra, K. K., and Kumar Bhardwaj, A.: Incidence of forest fire in India and its effect on terrestrial ecosystem
1056   dynamics, nutrient and microbial status of soil, International Journal of Agriculture and Forestry, 5(2), 69-
1057   78doi:10.5923/j.ijaf.20150502.01, 2015.

1058

1059   Chang, Y., Huang, R.J., Ge, X., Huang, X., Hu, J., Duan, Y., Zou, Z., Liu, X., and Lehmann, M. F.: Puzzling haze
1060   events in China during the coronavirus (COVID-19) shutdown. Geophys. Res. Lett., 47, e2020GL088533,
1061   doi:10.1029/2020GL088533, 2020.

1062

1063   Clark, H., Bennouna, Y., Tsivlidou, M., Wolff, P., Sauvage, B., Barret, B., Le Flochmoën, E., Blot, R., Boulanger, D.,
1064   Cousin, J.-M., Nédélec, P., Petzold, A., and Thouret, V.: The effects of the COVID-19 lockdowns on the composition
1065   of the troposphere as seen by In-service Aircraft for a Global Observing System (IAGOS) at Frankfurt, Atmos. Chem.
1066   Phys., 21, 16237–16256, https://doi.org/10.5194/acp-21-16237-2021, 2021.

1067

1068   Collivignarelli, M. C., Abba, A., Bertanza, G., Pedrazzani, R., Ricciardi, P., and Miino, M. C.: Lockdown for Covid-
1069   2019 in Milan: What are the effects on air quality?, Sci. Total Environ., 732, 139280,
1070   doi:10.1016/j.scitotenv.2020.139280, 2020.

1071

1072   Collyns, D.: Peru's coronavirus response was 'right on time' – so why isn't it working?, The Guardian,
1073   https://www.theguardian.com/global-development/2020/may/20/peru-coronavirus-lockdown-new-cases, last access:
1074   17 June 2020, 2020.

1075

1076   Conforti K.: Alert Level 2 restrictions to begin in New Zealand this week,
1077   https://www.forbes.com/sites/kaeliconforti/2020/05/13/alert-level-2-restrictions-to-begin-in-new-zealand-this-
1078   week/#52517b326497, last access: 17 June 2020, 2020.

1079

1080   Copernicus Sentinel-5P (processed by ESA): TROPOMI Level 2 Nitrogen Dioxide total column products. Version
1081   01. European Space Agency, doi:10.5270/S5P-s4ljg54, 2018a.

1082

1083   Copernicus Sentinel-5P (processed by ESA): TROPOMI Level 2 Carbon Monoxide total column products. Version
1084   01. European Space Agency, doi:10.5270/S5P-1hkp7rp, 2018b.

1085

1086   Copernicus Sentinel-5P (processed by ESA): TROPOMI Level 2 Formaldehyde Total Column products. Version 01.
1087   European Space Agency, doi:10.5270/S5P-tjlxfd2, 2018c.

1088

1089   Dattakiran, J.: Impact of lockdown on India's electricity sector, EnergyA, http://www.energy-a.eu/impact-of-ongoing-
1090   lockdown-on-indias-electricity-sector-an-overview/, last access: 9 June 2020, 2020.

1091

1092   De Smedt, I., Theys, N., Yu, H., Danckaert, T., Lerot, C., Compernolle, S., Van Roozendael, M., Richter, A., Hilboll,
1093   A., Peters, E., Pedergnana, M., Loyola, D., Beirle, S., Wagner, T., Eskes, H., van Geffen, J., Boersma, K. F., and
1094   Veefkind, P.: Algorithm theoretical baseline for formaldehyde retrievals from S5P TROPOMI and from the QA4ECV
1095   project, Atmos. Meas. Tech., 11, 2395–2426, doi:10.5194/amt-11-2395-2018, 2018.

1096

1097   De Smedt, I., Romahn, F., and Eichmann, K.-U.: S5P Mission Performance Centre Formaldehyde [L2__HCHO___]
1098   Readme, document number: S5P-MPC-BIRA-PRF-HCHO, 2.1, BIRA-IASB Royal Belgian Institute for Space
1099   Aeronomy, Brussels, Belgium, https://sentinels.copernicus.eu/web/sentinel/technical-guides/sentinel-5p/products-
1100   algorithms, 2020a.

1101

1102   De Smedt, I., Theys, N., Yu, H., Vlietinck, J., Lerot, C., and Van Roozendael, M.: S5P/TROPOMI HCHO ATBD,
1103   document number: S5P-BIRA-L2-400F-ATBD, 2.2.0, BIRA-IASB Royal Belgian Institute for Space Aeronomy,
1104   Brussels, Belgium, https://sentinels.copernicus.eu/web/sentinel/technical-guides/sentinel-5p/products-algorithms,
1105   2020b.

1106

1107   Diamond, M. S. and Wood, R.: Limited regional aerosol and cloud microphysical changes despite unprecedented

1108   decline in nitrogen oxide pollution during the February 2020 COVID-19 shutdown in China, Geophys. Res. Lett., 47,

1109   doi:10.1029/2020GL088913, 2020.

1110

1111   Dimitropoulou, E., Hendrick, F., Pinardi, G., Friedrich, M. M., Merlaud, A., Tack, F., De Longueville, H., Fayt, C.,

1112   Hermans, C., Laffineur, Q., Fierens, F., and Van Roozendael, M.: Validation of TROPOMI tropospheric NO_2 columns

1113   using dual-scan multi-axis differential optical absorption spectroscopy (MAX-DOAS) measurements in Uccle,

1114   Brussels, Atmos. Meas. Tech., 13, 5165–5191, doi:10.5194/amt-13-5165-2020, 2020.

1115

1116   Ding, J., van der A, R. J., Eskes, H. J., Mijling, B., Stavrakou, T., van Geffen, J. H. G. M., and Veefkind, J. P.: NOx

1117   emissions reduction and rebound in China due to the COVID-19 crisis. Geophys. Res. Lett., 46, e2020GL089912,

1118   doi.org:10.1029/2020GL089912, 2020.

1119

1120   Do Rosario, J., Gillespie P.: Argentina orders 'exceptional' Lockdown in bid to stem virus,

1121   https://www.bloomberg.com/news/articles/2020-03-20/argentina-orders-exceptional-lockdown-in-bid-to-contain-

1122   virus, last access: 17 June 2020, 2020.

1123

1124   Sentinel-5P Pre-Operations Data Hub: https://s5phub.copernicus.eu/, last access: 18 June 2021.

1125

1126   Eskes, H. J. and Boersma, K. F.: Averaging kernels for DOAS total-column satellite retrievals, Atmos. Chem. Phys.,

1127   3, 1285–1291, doi:10.5194/acp-3-1285-2003, 2003.

1128

1129   Eskes, H., van Geffen, J., Boersma, K. F., Eichmann, K.-U., Apituley, A., Pedergnana, M., Sneep, M., Veefkind, J.

1130   P., and Loyola, D.: Sentinel-5 precursor/TROPOMI Level 2 Product User Manual Nitrogendioxide, document

1131   number: S5P-KNMI-L2-0021-MA, 4.0.0, Royal Netherlands Meteorological Institute, De Bilt, The Netherlands,

1132   https://sentinels.copernicus.eu/web/sentinel/technical-guides/sentinel-5p/products-algorithms, 2020.

1133

1134   Eskes, H. J., and Eichmann, K.-U.: S5P Mission Performance Centre Nitrogen Dioxide [L2__NO2___] Readme,

1135   document number: S5P-MPC-KNMI-PRF-NO2, 1.6, Royal Netherlands Meteorological Institute, De Bilt, The

1136   Netherlands, https://sentinels.copernicus.eu/web/sentinel/technical-guides/sentinel-5p/products-algorithms, 2020.

1137

1138   Forster, P. M., Forster, H. I., Evans, M. J., Gidden, M. J., Jones, C. D., Keller, C. A., Lamboll, R. D., Le Quéré, C.,

1139   Rogelj, J., Rosen, D., Schleussner, C.-F., Richardson, T. B., Smith C. J., and Turnock, S. T.: Current and future global

1140   climate impacts resulting from COVID-19, Nat. Clim. Chang., 10, 913–919, doi:10.1038/s41558-020-0883-0, 2020.

1141

1142   Fioletov, V. E., McLinden, C. A., Krotkov, N., Li, C., Joiner, J., Theys, N., Carn, S., and Moran, M. D.: A global

1143   catalogue of large SO_2 sources and emissions derived from the Ozone Monitoring Instrument, Atmos. Chem. Phys.,

1144   16, 11497–11519, doi:10.5194/acp-16-11497-2016, 2016.

1145

1146   Fioletov, V., McLinden, C. A., Griffin, D., Theys, N., Loyola, D. G., Hedelt, P., Krotkov, N. A., and Li, C.:

1147   Anthropogenic and volcanic point source SO_2 emissions derived from TROPOMI on board Sentinel-5 Precursor: first

1148   results, Atmos. Chem. Phys., 20, 5591–5607, doi:10.5194/acp-20-5591-2020, 2020.

1149

1150   Fu, T.-M., Jacob, D. J., Wittrock, F., Burrows, J. P., Vrekoussis, M., and Henze, D. K.: Global budgets of atmospheric

1151   glyoxal and methylglyoxal, and implications for formation of secondary organic aerosols, J. Geophys. Res., 113,

1152   D15303, doi:10.1029/2007JD009505, 2008.

1153

1154   van Geffen, J. H. G. M., Eskes, H. J., Boersma, K. F., Maasakkers, J. D., and Veefkind, J. P.: TROPOMI ATBD of

1155   the total and tropospheric NO_2 data products, document number: S5P-KNMI-L2-0005-RP, 1.4.0, Royal Netherlands

1156   Meteorological Institute, De Bilt, The Netherlands, 2019.

1157

1158   van Geffen, J., Boersma, K. F., Eskes, H., Sneep, M., ter Linden, M., Zara, M., and Veefkind, J. P.: S5P TROPOMI

1159 NO_2 slant column retrieval: method, stability, uncertainties and comparisons with OMI, Atmos. Meas. Tech., 13,

1160   1315–1335, doi:10.5194/amt-13-1315-2020, 2020.

1161

1162   van Geffen, J. H. G. M., Eskes, H. J., Boersma, K. F., and Veefkind, J. P.: TROPOMI ATBD of the total and

1163   tropospheric NO_2 data products, document number: S5P-KNMI-L2-0005-RP, 2.2.0, Royal Netherlands

1164   Meteorological Institute, De Bilt, The Netherlands, https://sentinels.copernicus.eu/web/sentinel/technical-

1165   guides/sentinel-5p/products-algorithms, 2021.

1166

1167   Gkatzelis, G. I., Gilman, J. B., Brown, S. S., Eskes, H., Gomes, A. R., Lange, A. C., McDonald, B. C., Peischl, J.,

1168   Petzold, A., Thompson, C. R., and Kiendler-Scharr, A.: The Global Impacts of COVID-19 Lockdowns on Urban Air

1169   Quality: A Critical Review and Recommendations, Elem. Sci. Anth., 9, doi:10.1525/elementa.2021.00176, 2021.

1170

1171   Goldberg, D. L., Lu, Z., Streets, D. G., de Foy, B., Griffin, D., McLinden, C. A., Lamsal, L. N., Nickolay A. Krotkov,

1172   N. A., and Eskes, H.: Enhanced Capabilities of TROPOMI NO_2: Estimating NOx from North American Cities and

1173   Power Plants, Environ. Sci. Technol., 53(21), 12594-12601, doi:10.1021/acs.est9b04488, 2019.

1174

1175   Goldberg, D. L., Anenberg, S. C., Griffin, D., McLinden, C. A., Lu, Z., and Streets, D. G.: Disentangling the impact

1176   of the COVID-19 lockdowns on urban NO_2 from natural variability, Geophys. Res. Lett., 47, e2020GL089269,

1177   doi:10.1029/2020GL089269, 2020.

1178

1179   Goodman, A.: De Moura H., and Rebaza C. After 7 weeks of lockdown, Spaniards can finally exercise outdoors --
1180   as death toll passes 25,000, https://edition.cnn.com/2020/05/02/europe/spain-lockdown-coronavirus-exercise-
1181   intl/index.html, last access: 17 June 2020, 2020.

1183   Granier, C., Darras, S., Denier van der Gon, H., Doubalova, J., Elguindi, N., Galle, B., Gauss, M., Guevara, M.,
1184   Jalkanen, J.-P., Kuenen, J., Liousse, C., Quack, B., Simpson, D., and Sindelarova, K.: The Copernicus Atmosphere
1185   Monitoring Service global and regional emissions (April 2019 version), Copernicus Atmosphere Monitoring Service
1186   (CAMS) Report, Laboratoire d'Aérologie, Toulouse, France, 54pp., doi:10.24380/d0bn-kx16, 2019.

1188   Guevara, M., Jorba, O., Soret, A., Petetin, H., Bowdalo, D., Serradell, K., Tena, C., Denier van der Gon, H., Kuenen,
1189   J., Peuch, V.-H., and Pérez García-Pando, C.: Time-resolved emission reductions for atmospheric chemistry modelling
1190   in Europe during the COVID-19 lockdowns, Atmos. Chem. Phys., 21, 773–797, https://doi.org/10.5194/acp-21-773-
1191   2021, 2021.

1193   Holloway, T., Levy, H., and Kasibhatla, P.: Global distribution of carbon monoxide, J. Geophys. Res., 105, D10,
1194   12123-12147, doi:10.1029/1999JD901173, 2000.

1196   Horowitz, J.: Italy Locks Down Much of the Country's North Over the Coronavirus,
1197   https://www.nytimes.com/2020/03/07/world/europe/coronavirus-italy.html, last access: 17 June 2020, 2020a.

1199   Horowitz, J.: Hope and Worry Mingle as Countries Relax Coronavirus Lockdowns,
1200   https://www.nytimes.com/2020/05/04/world/europe/coronavirus-restrictions.html, last access: 17 June 2020, 2020b.

1202   Huang, G. and Sun, K.: Non-negligible impacts of clean air regulations on the reduction of tropospheric NO_2 over
1203   East China during the COVID-19 pandemic observed by OMI and TROPOMI, Sci. Total Environ., 745, 141023,
1204   doi:10.1016/j.scitotenv.2020.141023, 2020.

1206   Ialongo, I., Virta, H., Eskes, H., Hovila, J., and Douros, J.: Comparison of TROPOMI/Sentinel-5 Precursor NO_2
1207   observations with ground-based measurements in Helsinki, Atmos. Meas. Tech., 13, 205–218, doi:10.5194/amt-13-
1208   205-2020, 2020.

1210   Jain, S. and Sharma, T.: Social and travel lockdown impact considering Coronavirus disease (COVID-19) on air
1211   quality in megacities of India: present benefits, future challenges and way forward, Aerosol Air Qual. Res., 20, 1222–
1212   1236, doi:10.4209/aaqr.2020.04.0171, 2020.

1214   Janssens-Maenhout, G., Crippa, M., Guizzardi, D., Dentener, F., Muntean, M., Pouliot, G., Keating, T., Zhang, Q.,
1215   Kurokawa, J., Wankmüller, R., Denier van der Gon, H., Kuenen, J. J. P., Klimont, Z., Frost, G., Darras, S., Koffi, B.,

and Li, M.: HTAP_v2.2: a mosaic of regional and global emission grid maps for 2008 and 2010 to study hemispheric transport of air pollution, Atmos. Chem. Phys., 15, 11411–11432, https://doi.org/10.5194/acp-15-11411-2015, 2015.

Jennings, R., Philippines allows soft post-lockdown reopening to avert dire economic fall, https://www.voanews.com/east-asia-pacific/philippines-allows-soft-post-lockdown-reopening-avert-dire-economic-fall, last access: 17 June 2020, 2020.

Judd, L. M., Al-Saadi, J. A., Szykman, J. J., Valin, L. C., Janz, S. J., Kowalewski, M. G., Eskes, H. J., Veefkind, J. P., Cede, A., Mueller, M., Gebetsberger, M., Swap, R., Pierce, R. B., Nowlan, C. R., Abad, G. G., Nehrir, A., and Williams, D.: Evaluating Sentinel-5P TROPOMI tropospheric NO_2 column densities with airborne and Pandora spectrometers near New York City and Long Island Sound, Atmos. Meas. Tech., 13, 6113–6140, doi:10.5194/amt-13-6113-2020, 2020.

Kharol, S. K., Fioletov, V., McLinden, C. A., Shephard, M. W., Sioris, C. E., Li, C., and Krotkov, N.A.: Ceramic industry at Morbi as a large source of SO_2 emissions in India, Atmos. Environ., 223, doi:10.1016/j.atmosenv.2019.117243, 2019.

Koukouli, M. E., Skoulidou, I., Karavias, A., Parcharidis, I., Balis, D., Manders, A., Segers, A., Eskes, H. and Van Geffen, J.: Sudden changes in nitrogen dioxide emissions over Greece due to lockdown after the outbreak of COVID-19, Atmos. Chem. Phys., 21(3), 1759–1774, doi:10.5194/acp-21-1759-2021, 2021.

Krol, M., Houweling, S., Bregman, B., van den Broek, M., Segers,A., van Velthoven, P., Peters, W., Dentener, F., and Bergamaschi, P.: The two-way nested global chemistry-transport zoom model TM5: algorithm and applications, Atmos. Chem. Phys., 5, 417–432, doi:10.5194/acp-5-417-2005, 2005.

Kroll, J. H., Heald, C. L., Cappa, C. D., Farmer, D. K., Fry, J. L., Murphy, J. G., and Steiner, A. L.: The complex chemical effects of COVID-19 shutdowns on air quality, Nat. Chem., 12, 777-779, doi:10.1038/s41557-020-0535-z, 2020.

Kumari, P., and Toshniwal, D.: Impact of lockdown measures during COVID-19 on air quality–a case study of India. Int. J. Environ. Heal. R., 1-8, doi:10.1080/09603123.2020.1778646, 2020.

Lambert, J.-C., S. Compernolle, K.-U. Eichmann, M. de Graaf, D. Hubert, A. Keppens, Q. Kleipool, B. Langerock, M.K. Sha, T. Verhoelst, T. Wagner, C. Ahn, A. Argyrouli, D. Balis, K.L. Chan, I. De Smedt, H. Eskes, A.M. Fjæraa, K. Garane, J.F. Gleason, F. Goutail, J. Granville, P. Hedelt, K.-P. Heue, G. Jaross, ML. Koukouli, J. Landgraf, R. Lutz, S. Nanda, S. Niemeijer, A. Pazmiño, G. Pinardi, J.-P. Pommereau, A. Richter, N. Rozemeijer, M. Sneep, D. Stein Zweers, N. Theys, G. Tilstra, O. Torres, P. Valks, J. van Geffen, C. Vigouroux, P. Wang, and M. Weber. S5P

1253   MPC Routine Operations Consolidated Validation Report series, Issue #09, document number: S5P-MPC-IASB-

1254   ROCVR-09.01.01-20201221, 9.01.01, Royal Belgian Institute for Space Aeronomy, Brussels, Belgium, http://mpc-

1255   vdaf.tropomi.eu/index.php?option=com_vdaf&view=showReport&format=rawhtml&id=45

1256   2020.

1257

1258   Landgraf, J., aan de Brugh, J., Scheepmaker, R., Borsdorff, T., Hu, H., Houweling, S., Butz, A., Aben, I., and

1259   Hasekamp, O.: Carbon monoxide total column retrievals from TROPOMI shortwave infrared measurements, Atmos.

1260   Meas. Tech., 9, 4955–4975, doi:10.5194/amt-9-4955-2016, 2016.

1261

1262   Landgraf, J., aan de Brugh, J., Scheepmaker, R. A., Borsdorff, T., Houweling, S., and Hasekamp, O. P.: Algorithm

1263   Theoretical Baseline Document for Sentinel-5 Precursor: Carbon Monoxide Total Column Retrieval, document

1264   number: SRON-S5P-LEV2-RP-002, 1.10, SRON Netherlands Institute for Space Research, Utrecht, The Netherlands,

1265   https://sentinels.copernicus.eu/web/sentinel/technical-guides/sentinel-5p/products-algorithms, 2018.

1266

1267   Landgraf, J., Borsdorff, T., Langerock, B., and Keppens, A.: S5P Mission Performance Centre Carbon Monoxide

1268   [L2__CO____] Readme, document number: S5P-MPC-SRON-PRF-CO, 1.5, SRON Netherlands Institute for Space

1269   Research,   Utrecht,   The   Netherlands,   https://sentinels.copernicus.eu/web/sentinel/technical-guides/sentinel-

1270   5p/products-algorithms, 2020.

1271

1272   Lee, C., Martin, R. V., van Donkelaar, A., Lee, H., Dickerson, R. R., Hains, J. C., Krotkov, N., Richter, A., Vinnikov,

1273   K., and Schwab, J. J.: SO_2 emissions and lifetimes: Estimates from inverse modeling using in situ and global, space-

1274   based (SCIAMACHY and OMI) observations, J. Geophys. Res., 116, D06304, doi:10.1029/2010JD014758, 2011.

1275

1276   Lee, J. D., Drysdale, W. S., Finch, D. P., Wilde, S. E., and Palmer, P. I.: UK surface NO_2 levels dropped by 42%

1277   during the COVID-19 lockdown: impact on surface O_3, Atmos. Chem. Phys., doi:10.5194/acp-2020-838, 2020.

1278

1279   Le Quéré, C., Jackson, R. B., Jones, M. W., Smith, A. J. P., Abernethy, S., Andrew, R. M., De-Gol, A. J., Willis, D.

1280   R., Shan, Y., Canadell, J. G., Friedlingstein, P., Creutzig F., and Peters, G. P.: Temporary reduction in daily global

1281 CO_2 emisisons during the COVID-19 forced confinement, Nat. Clim. Chang., 10, 647-653, doi:10.1038/s41558-020-

1282   0797-x, 2020.

1283

1284   Lerot, C., Stavrakou, T., De Smedt, I., Müller, J.-F., and Van Roozendael, M.: Glyoxal vertical 576 columns from

1285   GOME-2 backscattered light measurements and comparisons with a global 577 model. Atmos. Chem. Phys. 10,

1286   12059-12072, 2010.

1287

1288 Lerot, C., Stavrakou, T., Van Roozendael, M., Alvarado, L. M. A., and Richter, A.: GLYoxal Retrievals from

1289 TROPOMI (GLYRETRO) ATBD, S5p+Innovation – theme 1 (CHOCHO), 5p+I_CHOCHO_BIRA_ATBD, issue

1290 2.1, 16 November 2020, https://glyretro.aeronomie.be/, 2020.

1291

1292 Leung, K., Wu, J. Liu, D., and Leung, G. M.: First-wave COVID-19 transmissibility and severity in China outside

1293 Hubei after control measures, and second-wave scenario planning: a modelling impact assessment, The Lancet, 395

1294 (10233), 1382-1393, doi:10.1016/S0140-6736(20)30746-7, 2020.

1295

1296 Li, C., McLinden, C., Fioletov, V., Krotkov, N., Carn, S., Joiner, J., Streets, D., He, H., Ren, X., Zhanqing Li, Z., and

1297 Dickerson, R. R.: India Is Overtaking China as the World's Largest Emitter of Anthropogenic Sulfur Dioxide, Sci.

1298 Rep., 7, 14304, doi:10.1038/s41598-017-14639-8, 2017.

1299

1300 Liu, F., Page, A., Strode, S. A., Yoshida, Y., Choi, S., Zheng, B., Lamsal, L. N., Li, C., Krotkov, N. A., Eskes, H.,

1301 van der A, R., Veefkind, P., Levelt, P. F., Hauser, O. P., and Joiner, J.: Abrupt decline in tropospheric nitrogen dioxide

1302 over China after the outbreak of COVID-19, Sci. Adv., 6, 28, eabc2992, doi:10.1126/sciadv.abc2992, 2020.

1303

1304 Lorente, A., Boersma, K. F., Eskes, H. J., Veefkind, J. P., van Geffen, J. H. G. M., de Zeeuw, M. B., Denier van der

1305 Gon, H. A. C., Beirle, S., and Krol, M. C.: Quantification of nitrogen oxides emissions from build-up of pollution over

1306 Paris with TROPOMI, Sci. Rep., 9, 20033, doi:10.1038/s41598-019-56428-5, 2019.

1307

1308 Loyola, D. G., Gimeno García, S., Lutz, R., Argyrouli, A., Romahn, F., Spurr, R. J. D., Pedergnana, M., Doicu, A.,

1309 Molina García, V., and Schüssler, O.: The operational cloud retrieval algorithms from TROPOMI on board Sentinel-

1310 5 Precursor, Atmos. Meas. Tech., 11, 409–427, doi:10.5194/amt-11-409-2018, 2018.

1311

1312 Ludewig, A., Kleipool, Q., Bartstra, R., Landzaat, R., Leloux, J., Loots, E., Meijering, P., van der Plas, E., Rozemeijer,

1313 N., Vonk, F., and Veefkind, P.: In-flight calibration results of the TROPOMI payload on board the Sentinel-5

1314 Precursor satellite, Atmos. Meas. Tech., 13, 3561–3580, doi:10.5194/amt-13-3561-2020, 2020.

1315

1316 Mahato, S., Pal, S., and Ghosh, K. G., Effect of lockdown amid COVID-19 pandemic on air quality of the megacity

1317 Delhi, India, Sci. Total Environ., 730, 139086, doi:10.1016/j.scitotenv.2020.139086, 2020.

1318

1319 Makooi, B.: Key points of France's strategy for lifting its nationwide Covid-19 lockdown.

1320 https://www.france24.com/en/20200429-key-points-of-france-s-strategy-for-lifting-its-nationwide-covid-19-

1321 lockdown, last access: 17 June 2020, 2020.

1322

1323 Masaki, T., Nakamura, S., Newhouse, D.: How is the COVID-19 crisis affecting nitrogen dioxide emissions in Sub-
1324 Saharan Africa? Poverty and Equity Notes, No. 21. World Bank, Washington, DC, World Bank.
1325 https://openknowledge.worldbank.org/handle/10986/33801, License: CC BY 3.0 IGO, 2020.

1327 Matthews, A.: Coronavirus: 5 things New Zealand got right, Deutsche Welle, https://p.dw.com/p/3dSVh, last access:
1328 2 July 2020, 2020.

1330 Mbah,   F.:   Businesses   reopen   as   Nigeria   eases   coronavirus   lockdown.   Available   from
1331 https://www.aljazeera.com/news/2020/05/businesses-reopen-nigeria-eases-coronavirus-lockdown-
1332 200504094440082.html, last access: 17 June 2020, 2020.

1334 Menon, P.:   'Stay at home' New Zealand PM urges ahead of coronavirus lockdown. Available from
1335 https://www.reuters.com/article/us-health-coronavirus-newzealand/stay-at-home-new-zealand-pm-urges-ahead-of-
1336 coronavirus-lockdown-idUSKBN21A3RN, last access: 17 June 2020, 2020.

1338 Millet, D. B., Jacob, D. J., Boersma, K. F., Fu, T. M., Kurosu, T. P., Chance, K., Heald, C. L., and Guenther, A.:
1339 Spatial distribution of isoprene emissions from North America derived from formaldehyde column measurements by
1340 the OMI satellite sensor, J. Geophys. Res., 113, D02307, doi:10.1029/2007jd008950, 2008.

1342 Minder, R. and Peltier, E.: Spain imposes nationwide lockdown to fight coronavirus. Available from
1343 https://www.nytimes.com/2020/03/14/world/europe/spain-coronavirus.html, last access: 17 June 2020, 2020.

1345 Misculin N., and Garrison C.: Argentina extends lockdown in Buenos Aires as coronavirus cases surpass 20,000.
1346 Available from https://www.thejakartapost.com/news/2020/06/05/argentina-extends-lockdown-in-buenos-aires-as-
1347 coronavirus-cases-surpass-20000.html, last access: 17 June 2020, 2020.

1349 Miyazaki, K., Bowman, K., Sekiya, T., Jiang, Z., Chen, X., Eskes, H., Ru, M., Zhang, Y., and Shindell, D.: Air
1350 quality response in China linked to the 2019 novel coronavirus (COVID-19) lockdown, Geophys. Res. Lett., 47,
1351 e2020GL089252, doi:10.1029/2020GL089252, 2020.

1353 Müller, J.-F., Stavrakou, T., Bauwens, M., Compernolle, S., and Peeters, J.: Chemistry and deposition in the Model
1354 of Atmospheric composition at Global and Regional scales using Inversion Techniques for Trace gas Emissions
1355 (MAGRITTE v1.0). Part B. Dry deposition, Geosci. Model Dev. Discuss., 1–49, doi:10.5194/gmd-2018-317, 2018.

1357 Müller, J.-F., Stavrakou, T., and Peeters, J.: Chemistry and deposition in the Model of Atmospheric composition at
1358 Global and Regional scales using Inversion Techniques for Trace gas Emissions (MAGRITTE v1.1) – Part 1:
1359 Chemical mechanism, Geosci. Model Dev., 12, 2307–2356, doi:10.5194/gmd-12-2307-2019, 2019.

1360

1361 Muñoz Sabater, J.: ERA5-Land monthly averaged data from 1981 to present, Copernicus Climate Change Service

1362 (C3S) Climate Data Store (CDS) [data set], last access: 09 June 2021, doi:10.24381/cds.68d2bb30, 2019a.

1363

1364 Muñoz Sabater, J.: ERA5-Land hourly averaged data from 1981 to present, Copernicus Climate Change Service (C3S)

1365 Climate Data Store (CDS) [data set], last access: 09 June 2021, doi:10.24381/cds.e2161bac, 2019b.

1366

1367 New South Wales Public Health: Public Health (COVID-19 Restrictions on Gathering and Movement) Order 2020,

1368 https://www.legislation.nsw.gov.au, last access: 2 July 2020, 2020.

1369

1370 Odunsi, P.: Africa: COVID-19 deaths hits 37,000, Nigeria on top 5, Daily Post Nigeria,

1371 https://dailypost.ng/2020/10/06/africa-covid-19-deaths-hits-37000-nigeria-on-top-5/, last access: 30 March 2021,

1372 2020.

1373

1374 Onishi, N. and Méheut, C.: Paris, a magnet for the world, becomes a ghost city after a lockdown takes effect. Available

1375 from https://www.nytimes.com/2020/03/17/world/europe/paris-coronavirus-lockdown.html, last access: 17 June

1376 2020, 2020.

1377

1378 Orjinmo, N.: Coronavirus lockdown: Nigerians cautious as restrictions eased in Lagos and Abuja. Available from

1379 https://www.bbc.com/news/world-52526923, last access: 17 June 2020, 2020.

1380

1381 Palmer, P. I., Jacob, D. J., Chance, K., Martin, R. V., Spurr, R. J. D., Kurosu, T. P., Bey, I., Yantosca, R., Fiore, A.,

1382 and Li, Q.: Air mass factor formulation for spectroscopic measurements from satellites: Application to formaldehyde

1383 retrievals from the Global Ozone Monitoring Experiment, J. Geophys. Res. Atmos., 106, D13, 14539–14550,

1384 doi:10.1029/2000JD900772, 2001.

1385

1386 Pasley, J.: Mexico has moved to 'Phase 3' — its most serious level of coronavirus alert — and faces a looming

1387 outbreak. Here's how it got to this point, https://www.insider.com/photo-mexico-coronavirus-move-to-phase-three-

1388 2020-4, last access: 17 June 2020, 2020.

1389

1390 Patel S.: When Is California Reopening? The New York Times. Available from

1391 https://www.nytimes.com/article/coronavirus-california-reopening-phases.html, last access: 17 June 2020, 2020.

1392

1393 POSOCO, Power System Operation Corporation Limited, National Load Despatch Centre: https://posoco.in/covid-

1394 19/, last access: 30 March 2021.

1395

1396   Prabhjote, G.: The most congested cities in India low lie vacant midst the nationwide lockdown, Business Insider

1397   India,   https://www.businessinsider.in/india/news/most-congested-cities-in-india-low-lie-vacant-midst-the-

1398   nationwide-lockdown/articleshow/75243376.cms, last access: 30 March 2021, 2020.

1399

1400   Qu, Z., Jacob, D. J., Silvern, R. F., Shah, V., Campbell, P. C., Valin, L. C. and Murray, L. T.: US COVID-19 shutdown

1401   demonstrates importance of background NO2 in inferring NOx emissions from satellite NO2 observations, Geophys.

1402   Res. Lett., 48(10), doi:10.1029/2021GL092783, 2021.

1403

1404   Raszewski, E., and Garrison, C.: Buenos Aires lockdown extended until June 7 after rise in coronavirus cases, Reuters,

1405   https://www.reuters.com/article/us-health-coronavirus-argentina/buenos-aires-lockdown-extended-until-june-7-

1406   after-rise-in-coronavirus-cases-idUSKBN22Z0YB?il=0, last access: 17 June 2020, 2020.

1407

1408   Romahn, F., Pedergnana, M., Loyola, D., Apituley, A., Sneep, M., Veefkind, J. P., De Smedt, I., and Chan, K. L.:

1409   Sentinel-5 precursor/TROPOMI Level 2 Product User Manual Formaldehyde HCHO, document number: S5P-L2-

1410   DLR-PUM-400F,   2.01.00,   DLR,   German   Aerospace   Center,   Oberpfaffenhofen,   Germany,

1411   https://sentinels.copernicus.eu/web/sentinel/technical-guides/sentinel-5p/products-algorithms, 2020.

1412

1413   Saleh, I.: Iraq locks down 6 districts in Baghdad to stem virus. Available from https://www.aa.com.tr/en/latest-on-

1414   coronavirus-outbreak/iraq-locks-down-6-districts-in-baghdad-to-stem-virus/1845104, last access: 17 June 2020,

1415   2020.

1416

1417   Sekiya, T., Miyazaki, K., Eskes, H., Sudo, K., Takigawa, M., and Kanaya, Y.: A comparison of the impact of

1418   TROPOMI and OMI tropospheric NO2 on global chemical data assimilation, Atmos. Meas. Tech. Discuss. [preprint],

1419   https://doi.org/10.5194/amt-2021-400, in review, 2021.

1420

1421   Shi, X. and Brasseur, G. P.: The response in air quality to the reduction of Chinese economic activities during the

1422   COVID-19 outbreak, Geophys. Res. Lett., 47, e2020GL088070, doi:10.1029/2020GL088070, 2020.

1423

1424   Singh, K. D., Goel, V., Kumar, H., and Gettleman, J.: India, Day 1: World's Largest Coronavirus Lockdown Begins,

1425   The   New   York   Times,   https://www.nytimes.com/2020/03/25/world/asia/india-lockdown-coronavirus.html,   last

1426   access: 30 March 2021, 2020.

1427

1428   Sonali P.: Australia's biggest state to ease coronavirus lockdown from May 15, https://www.reuters.com/article/us-

1429   health-coronavirus-australia/australias-biggest-state-to-ease-coronavirus-lockdown-from-may-15-

1430   idUSKBN22M01U, last access: 17 June 2020, 2020.

1431

Spurr R., and Christi M.: The LIDORT and VLIDORT Linearized Scalar and Vector Discrete Ordinate Radiative Transfer Models: Updates in the Last 10 Years. In: Kokhanovsky A. (eds) Springer Series in Light Scattering. Springer Series in Light Scattering. Springer, Cham., doi:10.1007/978-3-030-03445-0_1, 2019.

Srikanta, S., Pilla, F., Basu, B., Sarkar Basu, A., Sarkar, K., Chakraborti, S., Kumar Joshi, P., Zhang, Q., Wang, Y., Bhatt, S., Bhatt, A., Jha, S., Keesstra, S., and Roy, P. S.: Examining the effects of forest fire on terrestrial carbon emission and ecosystem production in India using remote sensing approaches, Sci. Tot. Environ., 725, doi:10.1016/j.scitotenv.2020.138331, 2020.

Stavrakou, T., Müller, J.-F., De Smedt, I., Van Roozendael, M., Kanakidou, M., Vrekoussis, M., Wittrock, F., Richter, A., and Burrows, J. P.: The continental source of glyoxal estimated by the synergistic use of spaceborne measurements and inverse modelling, Atmos. Chem. Phys., 9, 8431–8446, doi:10.5194/acp-9-8431-2009, 2009.

Stavrakou, T., Müller, J.-F., Bauwens, M., De Smedt, I., Van Roozendael, M., and Guenther, A. B.: Impact of short-term climate variability on volatile organic compounds emissions assessed using OMI satellite formaldehyde observations. Geophys. Res. Lett., 45, 8681– 8689, doi:10.1029/2018GL078676, 2018.

Stavrakou, T., Müller, J.-F., Bauwens, M., Doumbia, T., Elguindi, N., Darras, S., Granier, C., DeSmedt, I., Lerot, C., Van Roozendael, M., Franco, B., Clarisse, L., Clerbaux, C., Coheur, P.-F., Liu, Y., Wang, T., Shi, X., Gaubert, B., Tilmes, S., and Brasseur, G.: Atmospheric Impacts of COVID-19 on NO_x and VOC Levels over China Based on TROPOMI and IASI Satellite Data and Modeling, Atmosphere, 12(8):946, https://doi.org/10.3390/atmos12080946, 2021.

Sun, W., Zhu, L., De Smedt, I., Bai, B., Pu, D., Chen, Y., Shu, L., Wang, D., Fu, T.-M., Wang, X., and Yang, X.: Global significant changes in formaldehyde (HCHO) columns observed from space at the early stage of the COVID-19 pandemic, Geophys. Res. Lett., 48, e2020GL091265, doi:10.1029/2020GL091265, 2021.

Tack, F., Merlaud, A., Iordache, M.-D., Pinardi, G., Dimitropoulou, E., Eskes, H., Bomans, B., Veefkind, P., and Van Roozendael, M.: Assessment of the TROPOMI tropospheric NO_2 product based on airborne APEX observations, Atmos. Meas. Tech., 14, 615–646, doi:10.5194/amt-14-615-2021, 2021.

Tan, P. H., Chou, C., Liang, J. Y., Chou, C. C. K., and Shiu, C. J.: Air pollution "holiday effect" resulting from the Chinese New Year, Atmos. Environ., 43(13), 2114–2124, doi:10.1016/j.atmosenv.2009.01.037, 2009.

The Star: Iraq on total lockdown until March 28 over virus fears, https://www.thestar.com.my/news/regional/2020/03/22/iraq-on-total-lockdown-until-march-28-over-virus-fears, last access: 17 June 2020, 2020.

1469

1470 Theys, N., Fioletov, V., Li, C., De Smedt, I., Lerot, C., McLinden, C., Krotkov, N., Griffin, D., Clarisse, L., Hedelt,

1471 P., Loyola, D., Wagner, T., Kumar, V., Innes, A., Ribas, R., Hendrick, F., Vlietinck, J., Brenot, H., and Van

1472 Roozendael, M.: A sulfur dioxide Covariance-Based Retrieval Algorithm (COBRA): application to TROPOMI reveals

1473 new emission sources, Atmos. Chem. Phys., 21, 16727–16744, https://doi.org/10.5194/acp-21-16727-2021, 2021.

1474

1475 Uchoa, P.: Brazil coronavirus: 'Our biggest problem is fake news', BBC, https://www.bbc.com/news/world-latin-

1476 america-52739734, last access: 17 June 2020, 2020.

1477

1478 Veefkind, J. P., Aben, I., McMullan, K., Forster, H., de Vries, J., Otter, G., Claas, J., Eskes, H. J., de Haan, J. F.,

1479 Kleipool, Q., van Weele, M., Hasekamp, O., Hoogeveen, R., Landgraf, J., Snel, R., Tol, P., Ingmann, P., Voors., R.,

1480 Kruizinge, B., Vink, R., Visser, H., and Levelt, P. F.: TROPOMI on the ESA Sentinel-5 Precursor: A GMES mission

1481 for global observations of the atmospheric composition for climate, air quality and ozone layer applications, Remote

1482 Sens. Environ., 120, 70-83, 2012.

1483

1484 Verhoelst, T., Compernolle, S., Pinardi, G., Lambert, J.-C., Eskes, H. J., Eichmann, K.-U., Fjæraa, A. M., Granville,

1485 J., Niemeijer, S., Cede, A., Tiefengraber, M., Hendrick, F., Pazmiño, A., Bais, A., Bazureau, A., Boersma, K. F.,

1486 Bognar, K., Dehn, A., Donner, S., Elokhov, A., Gebetsberger, M., Goutail, F., Grutter de la Mora, M., Gruzdev, A.,

1487 Gratsea, M., Hansen, G. H., Irie, H., Jepsen, N., Kanaya, Y., Karagkiozidis, D., Kivi, R., Kreher, K., Levelt, P. F.,

1488 Liu, C., Müller, M., Navarro Comas, M., Piters, A. J. M., Pommereau, J.-P., Portafaix, T., Prados-Roman, C.,

1489 Puentedura, O., Querel, R., Remmers, J., Richter, A., Rimmer, J., Rivera Cárdenas, C., Saavedra de Miguel, L.,

1490 Sinyakov, V. P., Stremme, W., Strong, K., Van Roozendael, M., Veefkind, J. P., Wagner, T., Wittrock, F., Yela

1491 González, M., and Zehner, C.: Ground-based validation of the Copernicus Sentinel-5P TROPOMI NO$_2$ measurements

1492 with the NDACC ZSL-DOAS, MAX-DOAS and Pandonia global networks, Atmos. Meas. Tech., 14, 481–510,

1493 doi:10.5194/amt-14-481-2021, 2021.

1494

1495 Vigouroux, C., Langerock, B., Bauer Aquino, C. A., Blumenstock, T., Cheng, Z., De Mazière, M., De Smedt, I.,

1496 Grutter, M., Hannigan, J. W., Jones, N., Kivi, R., Loyola, D., Lutsch, E., Mahieu, E., Makarova, M., Metzger, J.-M.,

1497 Morino, I., Murata, I., Nagahama, T., Notholt, J., Ortega, I., Palm, M., Pinardi, G., Röhling, A., Smale, D., Stremme,

1498 W., Strong, K., Sussmann, R., Té, Y., van Roozendael, M., Wang, P., and Winkler, H.: TROPOMI–Sentinel-5

1499 Precursor formaldehyde validation using an extensive network of ground-based Fourier-transform infrared stations,

1500 Atmos. Meas. Tech., 13, 3751–3767, doi:10.5194/amt-13-3751-2020, 2020.

1501

1502 Wahlquist, C.: Australia's coronavirus lockdown – the first 50 days,

1503 https://www.theguardian.com/world/2020/may/02/australias-coronavirus-lockdown-the-first-50-days, last access: 17

1504 June 2020, 2020.

Wang, Y., Yuan, Y., Wang, Q., Liu, C. G., Zhi, Q., and Cao, J.: Changes in air quality related to the control of coronavirus in China: Implications for traffic and industrial emissions, Sci. Total Environ., 731, 139133, doi:10.1016/j.scitotenv.2020.139133, 2020.

Wang, Z., Zheng, F., Zhang, W., and Wang, S.: Analysis of SO_2 Pollution Changes of Beijing-Tianjin-Hebei Region over China Based on OMI Observations from 2006 to 2017, Adv. Meteorol., 2018, doi:10.1155/2018/8746068, 2018.

Williams, J. E., Boersma, K. F., Le Sager, P., and Verstraeten, W. W.: The high-resolution version of TM5-MP for optimized satellite retrievals: description and validation, Geosci. Model Dev., 10, 721–750, doi:10.5194/gmd-10-721-2017, 2017.

Winter, S.: Ramaphosa announces 21 day coronavirus lockdown for South Africa, https://businesstech.co.za/news/government/383927/ramaphosa-announces-21-day-coronavirus-lockdown-for-south-africa/, last access: 17 June 2020, 2020.

Zhang, R., Zhang, Y., Lin, H., Feng, X., Fu, T.-M., and Wang, Y.: NOx Emission Reduction and Recovery during COVID-19 in East China, Atmosphere (Basel)., 11(4), 433, doi:10.3390/atmos11040433, 2020.

Zhang, Z., Arshad, A., Zhang, C., Hussain, S. and Li, W.: Unprecedented Temporary Reduction in Global Air Pollution Associated with COVID-19 Forced Confinement: A Continental and City Scale Analysis, Remote Sens., 12(15), 2420, doi:10.3390/rs12152420, 2020.

Zhao, N., G. Wang, G. Li, J. Lang and H. Zhang: Air pollution episodes during the COVID-19 outbreak in the Beijing–Tianjin–Hebei region of China: An insight into the transport pathways and source distribution. Environmental Pollution 267, 115617, https://doi.org/10.1016/j.envpol.2020.115617, 2020.

Zhao, Y., Zhang, K., Xu, X., Shen, H., Zhu, X., Zhang, Y., Hu, Y. and Shen, G.: Substantial Changes in Nitrogen Dioxide and Ozone after Excluding Meteorological Impacts during the COVID-19 Outbreak in Mainland China, Environ. Sci. Technol. Lett., 7(6), 402–408, doi:10.1021/acs.estlett.0c00304, 2020.

Zheng, B., Tong, D., Li, M., Liu, F., Hong, C., Geng, G., Li, H., Li, X., Peng, L., Qi, J., Yan, L., Zhang, Y., Zhao, H., Zheng, Y., He, K., and Zhang, Q.: Trends in China's anthropogenic emissions since 2010 as the consequence of clean air actions, Atmos. Chem. Phys., 18(19), 14095–14111, doi:10.5194/acp-18-14095-2018, 2018a.

Zheng, B., Chevallier, F., Ciais, P., Yin, Y., Deeter, M. N., Worden, H. M., Wang, Y., Zhang, Q., and He, K.: Rapid decline in carbon monoxide emissions and export from East Asia between years 2005 and 2016, Environ. Res. Lett., 13(4), doi:10.1088/1748-9326/aab2b3, 2018b.

1542   Zhu, L., Mickley, L. J., Jacob, D. J., Marais, E. A., Sheng, J., Hu, L., Abad, G. G., and Chance, K.: Long-term (2005–

1543   2014) trends in formaldehyde (HCHO) columns across North Americas seen by the OMI satellite instrument:

1544   Evidence of changing emissions of volatile organic compounds, Geophys. Res. Lett., 44, 7079–7086,

1545   doi:10.1002/2017GL073859, 2017.